Molecular Intracage Chemistry: $[Rh_6(CO)_{15}]^{2-}$ in Zeolite NaX

W. A. Weber, B. L. Phillips, and B. C. Gates*[a]

Abstract: $[Rh_6(CO)_{15}]^{2-}$ was made by ship-in-a-bottle synthesis in the cages of zeolite NaX by carbonylation of sorbed $[Rh(CO)_2(acac)]$ at 125 °C and was identified by ^{13}C NMR, infrared, and extended X-ray absorption fine structure (EXAFS) spectra. The ^{13}C NMR data indicate yields of $[Rh_6(CO)_{15}]^{2-}$ up to about 83 % in the cages. The synthesis chemistry is analogous to that in basic solutions. The NMR and infrared results indicate that, at room temperature, cluster–zeolite interactions are strong and CO intraexchange negligible, whereas at 80 °C these interactions are weak, allowing rapid intraexchange of CO ligands on the metal frame. Decarbonylation in H_2 at 200 °C gave partially decarbonylated clusters with a Rh–Rh first-shell coordination number matching that of $[Rh_6(CO)_{15}]^{2-}$, indicating that the metal frame remained nearly intact; decarbonylation at higher temperatures gave aggregated rhodium. The partially decarbonylated clusters formed in H_2 at 200 °C (or rhodium subcarbonyl fragments formed by oxidation in air at 25 °C) were reversibly recarbonylated to give $[Rh_6(CO)_{15}]^{2-}$. Treatment in He at 200–300 °C gave fully decarbonylated clusters with a Rh–Rh first-shell coordination number of about 2.6, suggesting that the cluster frames were intact but slightly flattened or fragmented. The decarbonylated rhodium clusters and aggregates catalyze toluene hydrogenation at temperatures of 80–120 °C. All this molecular chemistry is inferred to have taken place in isolated zeolite cages.

Keywords: clusters · rhodium · supramolecular chemistry · zeolites

Introduction

Molecular-scale cages, such as those in crystalline aluminosilicate zeolites, provide new environments for chemistry, even in the absence of solvents. Entrapment in cages allows investigation of isolated molecules and ions.[1, 2] Synthesis in a zeolite cage is called ship-in-a-bottle synthesis when the molecule formed is too large to pass through the windows connecting the cages, for example, in faujasites (zeolites X and Y). An illustration of this is the synthesis of manganese complexes in zeolite NaY[3] to form potential chiral catalysts. Isolation of molecules in cages can eliminate bimolecular interactions and thereby stabilize coordinative unsaturation and facilitate catalysis. Platinum clusters in zeolite LTL are used commercially as catalysts for naphtha reforming.[4] Purification of entrapped species is hardly possible, nor is their identification by classical methods, because extraction would require destruction of the zeolite, which may lead to changes in the species released from the cages. Consequently, researchers have relied on spectroscopic methods to investigate the chemistry of intracage species, and synthetic-yield data are lacking. Development of molecular chemistry in cages requires further advances in the application of quantitative spectroscopic methods for characterization of the entrapped species. Here we demonstrate the value of ^{13}C NMR spectroscopy for elucidation of intrazeolite organometallic chemistry, reporting the first well-defined anionic metal clusters in cages, $[Rh_6(CO)_{15}]^{2-}$ in zeolite NaX, with yield data and evidence of cluster decarbonylation with little change in nuclearity, giving catalysts for toluene hydrogenation.

[a] Prof. B. C. Gates,[+] W. A. Weber, B. L. Phillips
Department of Chemical Engineering and Materials Science
University of California, Davis, CA 95616

[+] Correspondence to this author at the following address:
Prof. Dr. Bruce C. Gates
Institut für Physikalische Chemie, Universität München
Butenandstrasse 5–13 (Haus E), D-81377 München (Germany)
Fax: (49) 89 2180-7605

Results

Formation of $[Rh_6(CO)_{15}]^{2-}$ in zeolite NaX

NMR evidence of $[Rh_6(CO)_{15}]^{2-}$: The intracage synthesis was carried out with $[Rh(CO)_2(acac)]$ ([dicarbonylacetylacetonato rhodium(I)]) in the pores of zeolite NaX; this precursor was chosen because it is small enough to diffuse readily from solution into the zeolite cages. In the room-temperature ^{13}C MAS-NMR spectrum of the sample formed by the carbonylation of $[Rh(CO)_2(acac)]$ in the uncalcined zeolite, most of the observed intensity is associated with three broad spinning side-band envelopes, with isotropic shifts $\delta = 203$, 230, and 258 (Figure 1A). The resonances occur in an approximate ratio of

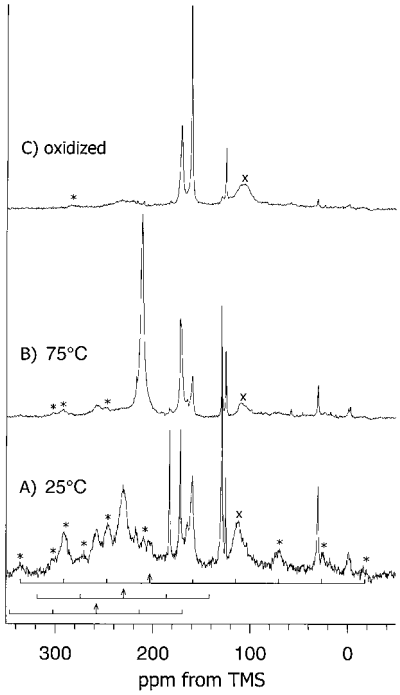

Figure 1. ^{13}C spin-echo MAS-NMR spectra of A) uncalcined zeolite NaX-supported rhodium carbonyls formed from $[Rh(CO)_2(acac)]$ in flowing CO at 2 bar and 125 °C for 12 h at 25 °C. Positions of spinning side-band envelopes with isotropic shifts $\delta = 203$, 230, and 258 are denoted by arrows below the spectrum. Data were obtained at 100.6 MHz with 4.4 kHz spinning rate, 225 μs interpulse delay (1 rotor period), 20 s relaxation period, and 4400 acquisitions. B) Same as in A), but at 75 °C; 7600 acquisitions. C) Sample of A) after oxidation in air. The spectrum was measured at 25 °C with a spinning rate of 5.0 kHz (200 μs interpulse delay), 20 s relaxation period, and 7000 acquisitions. Features marked by "*" are spinning sidebands; "X" denotes background signal from sample probe/rotor assemblies.

4:2:1, respectively (but the intensities might not accurately reflect abundances because of differences in T_1 and T_2); the spectrum also includes narrow peaks in the range for CO at $\delta = 160$, 165, 172, and 183, with other minor peaks characterized by smaller chemical shifts[5] (Table 1). Spectra measured at 75 °C (Figure 1B) show that most of the broad spinning side-band intensity observed at room temperature collapses into a single peak at $\delta = 211$. This new peak first appeared at temperatures between 20 and 45 °C and increased in intensity gradually with temperature, with simultaneous decreases in the intensities of the peaks at $\delta = 203$, 230, and 258 and their associated spinning sidebands; these intensities declined almost to zero at the highest temperature investigated, 90 °C. The spectrum recorded upon cooling of the sample from 75 °C back to room temperature was indistinguishable from that measured originally at room temperature, except for a decrease in the intensity of the $\delta = 183$ peak.

Oxidation of the sample formed by carbonylation of $[Rh(CO)_2(acac)]$ in uncalcined zeolite resulted in a spectrum characterized by three main peaks, at $\delta = 171.6$, 161, and 125, with a minor broad peak at $\delta = 230$ (Figure 1C). The peaks at $\delta = 171.6$ and 161 are consistent with rhodium subcarbonyls,[16–18] $\{Rh^I(CO)_2\}$, in which the Rh is bonded to oxygen atoms of the zeolite. The isotropic nature of these peaks indicates fluxionality of the CO ligands.

The ^1H MAS-NMR spectrum (Figure 2) of the sample prepared by the carbonylation of $[Rh(CO)_2(acac)]$ in the uncalcined zeolite at 125 °C, recorded at room temperature, shows no evidence of hydride ligands, which would be evident at about $\delta = -15$.[9, 19] Thus, the peaks at $\delta = 258$, 230, and 203 in the room-temperature spectrum (Figure 1A) are attributed to rhodium carbonyls without hydride ligands. The reversible

Table 1. Summary of ^{13}C NMR and ^1H NMR spectra: rhodium carbonyl complexes in solution and in zeolites NaY and NaX.

Metal carbonyl	^{13}C isotropic shifts δ [ppm]	^1H isotropic shifts δ [ppm]	Temperature [°C]	Ref.
$[Rh(CO)_2(acac)]$ in uncalcined zeolite NaX treated in CO at 125 °C and 2 bar for 12 h	major: 258, 230, 203, 183, 172, 160 minor: 139, 125, 24.7, 22.6, 13.1	–	−80	this work
$[Rh(CO)_2(acac)]$ in uncalcined zeolite NaX treated in CO at 125 °C and 2 bar for 12 h	major: 258, 230, 203, 183, 172, 160 minor: 139, 125, 24.7, 22.6, 13.1	–	25	this work
$[Rh(CO)_2(acac)]$ in uncalcined zeolite NaX treated in CO at 125 °C and 2 bar for 12 h	major: 211, 183, 172, 160 minor: 139, 125, 24.7,22.6, 13.1	–	75	this work
$[Rh(CO)_2(acac)]$ in uncalcined zeolite NaY treated in CO at 125 °C and 2 bar for 12 h and subsequently oxidized in air at room temperature	major: 230, 171.6, 161.0, 125.3 minor: 218, 210, 182.9, 129.4	–	25	this work
$[Na(CO)_2(acac)]$ in uncalcined zeolite NaY treated in CO at 125 °C and2 bar for 12 h	139, 34.7, 22.6, 13.1	–	25	this work
$[Rh_6(CO)_{15}]^{2-}$in zeolite NaX	258, 230, 203	–	25	this work
$[Rh_6(CO)_{15}]^{2-}$in zeolite NaX	211	–	75	this work
$[Rh_6(CO)_{15}]^{2-}$in perdeuterioacetone	209.2	–	−70	6
$[Rh_6(CO)_{15}C]^{2-}$in perdeuterioacetone	(264) 236, 224, 206, 196	–	−70	7
$[Rh_6(CO)_{16}]$ in $CDCl_3$	231.5, 180.1	–	70	6
$Rh(CO)_2(acac)$ in CH_2Cl_2	183.8	–	–	8
$[Rh_6H(CO)_{15}]^-$in perdeuterioacetone	244.6, 237.5, 232.9, 191.8, 187.1 183.6, 184.6	−12.2	−70	9
$[Rh_6H(CO)_{15}C]^-$ in acetone	(291.2) 225.1, 223.5, 216.0, 193.3, 189.6	−15.6	−25	9
$[Rh_4(CO)_{12}]$ in CD_2Cl_2	228.8, 183.4, 181.8, 175.5	–	−65	10,11
$[Rh_4(CO)_{11}(PMePh_3)]$ in CD_2Cl_2	235.9, 234.8, 184.4, 181.7, 178.9	–	−55	12
$[Rh_6(CO)_{15}I]^-$in CD_2Cl_2	245.3, 239.2, 232.9, 183.3	–	−60	12
$[Rh_7(CO)_{16}]^{3-}$in CD_2Cl_2	254.3, 229.5, 218.1, 206.4, 205.7, 198.2	–	−30	13
$[Rh_6H(CO)_{13}C]^{2-}$in THF	(460.4) 231.7, 235.7, 215.5, 209.0, 195.2, 193.6, 192.2	−14.6	−100	14
$[Rh_6(CO)_{13}C]^{2-}$in THF	(470) 242.5, 207.7, 202.4	–	−96	7
$[Rh_5(CO)_{15}]^-$in perdeuterioacetone	247.7, 207.9, 190.6	–	−80	15
$[Rh_6(CO)_{14}]^{4-}$in $CDCl_3$	252.9, 207	–	−72	6

0947-6539/99/0510-2900 $ 17.50+.50/0 *Chem. Eur. J.* **1999**, *5*, No. 10

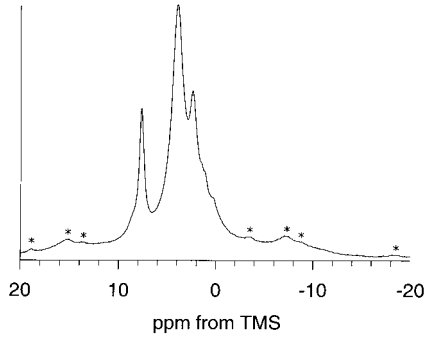

Figure 2. ^{1}H MAS-NMR spectrum of uncalcined zeolite NaX-supported rhodium carbonyls formed from $[Rh(CO)_2(acac)]$ in flowing CO at 2 bar and 125 °C for 12 h obtained at 400.1 MHz (single pulse excitation, 4.5 kHz spinning rate, 1.5 s relaxation delay, 400 acquisitions). Features marked by "*" are spinning sidebands.

replacement of the three spinning side-band envelopes with a single peak (at $\delta = 211$) with increasing temperature indicates that the resonances arise from a single rhodium species that undergoes complete CO intraexchange on the NMR time-scale (ca. 1 ms) at elevated temperature.

The rhodium carbonyl peaks observed at room temperature are not sufficient to identify the supported species; they are consistent with the solution ^{13}C NMR spectra of either $[Rh_7(CO)_{16}]^{3-}$ or $[Rh_6(CO)_{15}C]^{2-}$ (Table 1), and even $[Rh_6(CO)_{15}]^{2-}$, because all reported solution ^{13}C NMR spectra of $[Rh_6(CO)_{15}]^{2-}$ display rapid intraexchange of all CO ligands. Both $[Rh_7(CO)_{16}]^{3-}$ and $[Rh_6(CO)_{15}]^{2-}$ incorporate edge- and face-bridging (in addition to terminal) CO ligands, consistent with the observation of resonances at $\delta = 256$, 230, and 203. For example, $[Rh_7(CO)_{16}]^{3-}$ in solution is characterized by peaks corresponding to edge-bridging ($\delta = 229.5$, 218), face-bridging ($\delta = 254$), and terminal ($\delta = 206.4$, 205.7, and 198.7) CO ligands.[6] $[Rh_6(CO)_{15}C]^{2-}$ has only terminal and edge-bridging CO ligands, but in solution the carbido carbon gives a chemical shift ($\delta = 264$) similar to that of the face-bridging CO in $[Rh_7(CO)_{16}]^{3-}$.[20]

The structural resolution is provided by the high-temperature ^{13}C NMR spectrum, which is consistent with only one of the candidate clusters, $[Rh_6(CO)_{15}]^{2-}$, because this is the only one that would undergo complete intraexchange of all the CO ligands. The evidence is as follows: 1) The chemical shift of $[Rh_6(CO)_{15}]^{2-}$ in perdeuterioacetone solution ($\delta = 209$)[6] almost exactly matches that observed for the zeolite-supported sample at 75 °C ($\delta = 211$); 2) the data are not consistent with the presence of $[Rh_6(CO)_{15}C]^{2-}$ because the interior carbido carbon atom (which would give a peak near $\delta = 250$[20]) is not accessible for exchange, and we have observed a peak for the carbido carbon atom in a similar sample.[21, 22] Although a small peak remained in this region at high temperature, its intensity decreased with increasing temperature (being very weak at 90 °C), and it occurs with spectral features associated with the $\delta = 230$ and 203 resonances. Thus, these peaks are assigned to still-frozen clusters in which CO intraexchange remains slow because of interactions with the zeolite (Figure 1A). 3) The data are not consistent with the presence of $[Rh_7(CO)_{16}]^{3-}$ because not all the CO ligands would undergo exchange in this cluster, as indicated by the solution spectra measured at various temperatures.[6, 14, 23]

The yields of $[Rh_6(CO)_{15}]^{2-}$ were calculated from the ^{13}C NMR intensity ratios in the 75 °C spectrum;[24] the yield in the uncalcined zeolite was about 83 %; that in the calcined zeolite was less.

Sample colors and infrared evidence of rhodium carbonyls: $[Rh(CO)_2(acac)]$ in uncalcined zeolite NaX, after removal of the pentane solvent from the slurry used in the preparation, was yellowish brown. A similar sample formed from calcined zeolite NaX was bright yellow. Each sample was characterized by an infrared spectrum with two strong $\tilde{\nu}_{CO}$ bands, at 2087 and 2006 cm^{-1}, consistent with the presence of rhodium dicarbonyl species[25–29] (Figure 3, Table 2).

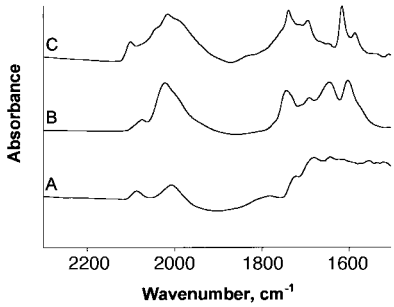

Figure 3. Infrared spectra of A) uncalcined zeolite NaX containing $[Rh(CO)_2(acac)]$; B) sample formed by treating A) in CO at 2 bar and 125 °C for 12 h; and C) sample formed in calcined zeolite NaX containing $[Rh(CO)_2(acac)]$, which had been treated in CO at 2 bar and 125 °C for 12 h.

Treatment of the uncalcined sample in flowing CO at 125 °C and 2 bar for 12 h gave a green solid with an infrared spectrum ($\tilde{\nu}_{CO}$ = 2074w, 2022vs, 1995sh, 1742s cm^{-1}; Table 2, Figure 3B) similar to that of $[Rh_6(CO)_{15}]^{2-}$, but not distinguishable from those of $[Rh_6(CO)_{15}C]^{2-}$ and $[Rh_7(CO)_{16}]^{3-}$ in solution (Table 2).[41, 43] The same treatment of the calcined sample led to a similar infrared spectrum ($\tilde{\nu}_{CO}$: 2100w, 2050sh, 2015s, 1995sh, 1738s cm^{-1}; Figure 3C). Comparison of the spectra shows that the intensity of the strongest $\tilde{\nu}_{CO}$ peak, near 2020 cm^{-1}, is greater in the spectrum of the uncalcined sample than in that of the calcined sample (Figure 3), consistent with the higher yield of $[Rh_6(CO)_{15}]^{2-}$ in the uncalcined zeolite.[44]

When the samples were exposed to air at room temperature, the spectra indicated an almost instantaneous oxidation to give the rhodium subcarbonyls accompanied by the disappearance of the rhodium carbonyl clusters. The $\tilde{\nu}_{CO}$ peaks and shoulders (2087, 2006 cm^{-1}) indicating the presence of rhodium subcarbonyls [e.g., supported $\{Rh^{I}(CO)_2\}$, bonded to oxygen atoms of the zeolite frame[25–28, 45]] are more intense in the spectrum of the calcined than the uncalcined zeolite; this corresponds to the lower yield of cluster in the former.

The sample formed by the carbonylation of $[Rh(CO)_2(acac)]$-containing zeolite NaX, whether or not it was calcined, was green. There are only two known rhodium carbonyl clusters that are green, $[Rh_6(CO)_{15}]^{2-}$ and $[Rh_7(CO)_{16}]^{3-}$. The samples containing rhodium subcarbonyls were brownish yellow.

Table 2. Summary of infrared spectra: ν_{CO}-stretching frequencies characterizing metal carbonyls in solution and in zeolites NaY and NaX.

Metal carbonyl	Terminal CO stretching frequency [cm^{-1}]	Bridging CO stretching frequency [cm^{-1}]	Ref.
$[Rh(CO)_2(acac)]$ in uncalcined zeolite NaX	2006s, 2087s		this work
$[Rh(CO)_2(acac)]$ in uncalcined zeolite NaY treated in CO at 125 °C and 2 bar for 12 h	2074w, 2022vs, 1995sh	1742s	this work
$[Rh_6(CO)_{16}]$ in zeolite NaY	2099s, 2069w, 2020w	1765s	30–32
$[Rh_6(CO)_{16}]$ in $CHCl_3$	2076s, 2046w	1805m	30
$[Rh_4(CO)_{12}]$ in zeolite NaY	2086vs, 2069sh, 2050sh, 2025sh	1834s	31,32
$[Ir_4(CO)_{12}]$ in THF	2110vw, 2067vs, 2026mw		33
$[Ir_4(CO)_{12}]$ in zeolite NaY	2115w, 2072s, 2034m		34
$[Ir_6(CO)_{16}]$ in CH_2Cl_2	2115w, 2075s, 2057sh, 2047w, 2034vw, 2009vw	1800w, 1765s	35
$[Ir_6(CO)_{16}]$ in zeolite NaY	2129w, 2096sh, 2084s, 2054w, 2039m	1818s	35,36
$[NEt_4][Ir_4(CO)_{11}]$ in THF	2067w, 2030sh, 2017vs, 1986m, 1978m	1832m	37
$[Ir_4(CO)_{11}]^-$in zeolite NaX	2072w, 2044sh, 2035s, 2011m, 2000sh	1765mw	38
$[NEt_4][Ir_6(CO)_{15}]$ in THF	2030sh, 19770s, 1910sh	1775s, 1735s	35
$[Ir_6(CO)_{15}]^{2-}$in zeolite NaX	2001s, 1993s	1710s	38
$[Ir_6(CO)_{15}]^{2-}$on γ-Al_2O_3	2067sh, 2040m, 2010vs	1837w	39
$[Ir_6(CO)_{15}]^{2-}$on MgO	2060m, 2012vs	1832w	33
$[PPN]_2[Rh_4(CO)_{11}]$ in THF	2075w, 2030vs, 2010s, 1995sh, 1965sh	1892w, 1845s	40
$[PPN][Rh_5(CO)_{15}]$ in THF	2043s, 2010vs	1871mw, 1942ms, 1787m	41
$[NMe_4]_3[Rh_7(CO)_{16}]$ in CH_3CN	2020w(sh), 1995w(sh), 1955s, 1954sh	1810w, 1770s, 1738w(br)	42

Lack of extraction indicating entrapment of rhodium carbonyls in zeolite: Attempts were made to extract rhodium carbonyls from the CO-treated zeolite samples with THF, $CHCl_3$, or CH_3CN, each with and without [PPN]Cl [bis(triphenylphosphine)iminium chloride]. Infrared spectra of these extract solutions gave no evidence of metal carbonyls, indicating that the rhodium carbonyls were large enough to be trapped in the zeolite cages (i.e., they were clusters) and/or that they were stably bound to the zeolite surface (e.g., they were rhodium subcarbonyls).

EXAFS evidence of cluster structures: The results of the EXAFS analysis, with details summarized in Table 3, show that the rhodium carbonyls formed in the uncalcined and the calcined zeolite, following treatment in CO (Figure 4), are characterized by oscillations up to values of k (the wavenumber) of about 16 $Å^{-1}$, consistent with Rh–Rh bonds and clusters. The data characterizing each of the samples were fitted as stated in the section below entitled "EXAFS data analysis". The structural parameters are summarized in Table 4, and comparisons of the data and the fits, in k space and in r space [r is the absorber (Rh)-scatterer distance], are shown in Figures 5A and B, respectively (only for the uncalcined zeolite).

The peaks at 2.6 Å in the Fourier transforms of the data (Figure 5) correspond to Rh–Rh contributions in clusters. The magnitude of this peak was greater for the uncalcined than for the calcined sample, indicating a larger average Rh–Rh coordination number for the rhodium carbonyls in the uncalcined zeolite, consistent with the higher yield of $[Rh_6(CO)_{15}]^{2-}$.

X-ray diffraction data[47] representing $[Rh_6(CO)_{15}I]^-$, which is expected to have a structure similar to that of $[Rh_6(CO)_{15}]^{2-}$ in the zeolite, show that each Rh atom is bonded to four Rh atoms at an average distance of 2.746 Å, to two terminal CO ligands (except for one Rh atom which is bonded to a terminal CO and an iodide ion), with an average Rh–C_t distance of 1.85 Å, and to two face-bridging CO ligands, with an average Rh–C_{fb} distance of 2.17 Å (where the subscripts t and fb refer to terminal and face-bridging, respectively). The EXAFS data characterizing $[Rh_6(CO)_{15}]^{2-}$ supported in the uncalcined zeolite (Table 4) also indicate that each Rh atom is bonded to

Table 3. Summary of EXAFS analysis: fitted k range and r range, number of scans, and standard deviation (SD) in EXAFS function for rhodium in zeolite NaX samples.

Sample	No. of scans	SD in EXAFS function[a]	k Range [$Å^{-1}$]	r Range, [Å]	P[b]
$[Rh_6(CO)_{15}]^{2-}$in uncalcined zeolite NaX	5	0.004	4.2–14.7	0–5	34
$[Rh_6(CO)_{15}]^{2-}$in calcined zeolite NaX	3	0.004	4.2–14.7	0–5	34
$[Rh_6(CO)_{15}]^{2-}$in uncalcined zeolite NaX after H_2 at 200 °C	2	0.001	4.1–14.7	0–5	34
$[Rh_6(CO)_{15}]^{2-}$in uncalcined zeolite NaX after H_2 at 250 °C	2	0.001	4.1–14.7	0–5	34
$[Rh_6(CO)_{15}]^{2-}$in uncalcined zeolite NaX after H_2 at 300 °C	2	0.001	4.1–14.7	0–5	34
$[Rh_6(CO)_{15}]^{2-}$in calcined zeolite NaX after H_2 at 200 °C	2	0.001	4.1–14.7	0–5	34
$[Rh_6(CO)_{15}]^{2-}$ in calcined zeolite NaX after H_2 at 250 °C	2	0.001	4.1–14.7	0–5	34
$[Rh_6(CO)_{15}]^{2-}$in calcined zeolite NaX after H_2 at 300 °C	2	0.001	4.1–14.7	0–5	34
$[Rh_6(CO)_{15}]^{2-}$in uncalcined zeolite NaX after He at 200 °C	2	0.001	4.1–14.7	0–5	34
$[Rh_6(CO)_{15}]^{2-}$in uncalcined zeolite NaX after He at 250 °C	2	0.001	4.1–14.7	0–5	34
$[Rh_6(CO)_{15}]^{2-}$in uncalcined zeolite NaX after He at 300 °C	2	0.001	4.1–14.7	0–5	34
$[Rh_6(CO)_{15}]^{2-}$in calcined zeolite NaX after He at 200 °C	2	0.001	4.1–14.7	0–5	34
$[Rh_6(CO)_{15}]^{2-}$in calcined zeolite NaX after He at 250 °C	2	0.001	4.1–14.7	0–5	34
$[Rh_6(CO)_{15}]^{2-}$in calcined zeolite NaX after He at 300 °C	2	0.001	4.1–14.7	0–5	34

[a] Calculated standard deviation from a similar sample that had been scanned six times. [b] Statistically justified number of free parameters that can be fitted. Calculated from the Nyquist theorem, $P = 2\Delta k\Delta r/\pi + 1$,[46] where Δk and Δr are the ranges in the wavenumber and distance from the absorber Rh atom.

0947-6539/99/0510-2902 $ 17.50+.50/0 *Chem. Eur. J.* **1999**, *5*, No. 10

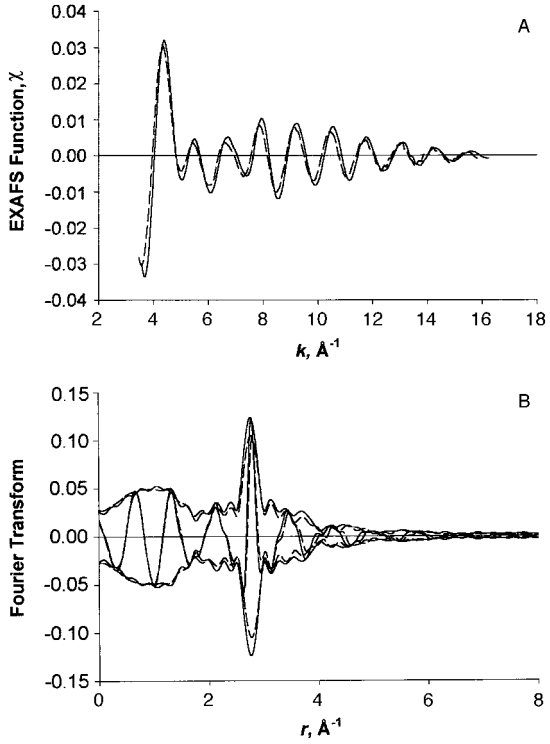

Figure 4. A) Raw EXAFS data characterizing uncalcined zeolite NaX-supported rhodium carbonyl clusters formed from $[Rh(CO)_2(acac)]$ in flowing CO at 125 °C and 2 bar for 12 h (solid line) and sample formed in calcined zeolite NaX (dashed line). B) Fourier transform (phase and amplitude corrected with data characterizing Rh foil) of the raw EXAFS data characterizing uncalcined zeolite NaX-supported rhodium carbonyl clusters formed from $[Rh(CO)_2(acac)]$ in flowing CO at 125 °C and 2 bar for 12 h (solid line) and sample formed in calcined zeolite NaX (dashed line).

about four Rh atoms, on average, at an average distance of 2.76 Å. The EXAFS data also indicate Rh–C contributions at 1.88 and 2.10 Å, in approximate agreement with the crystallo-

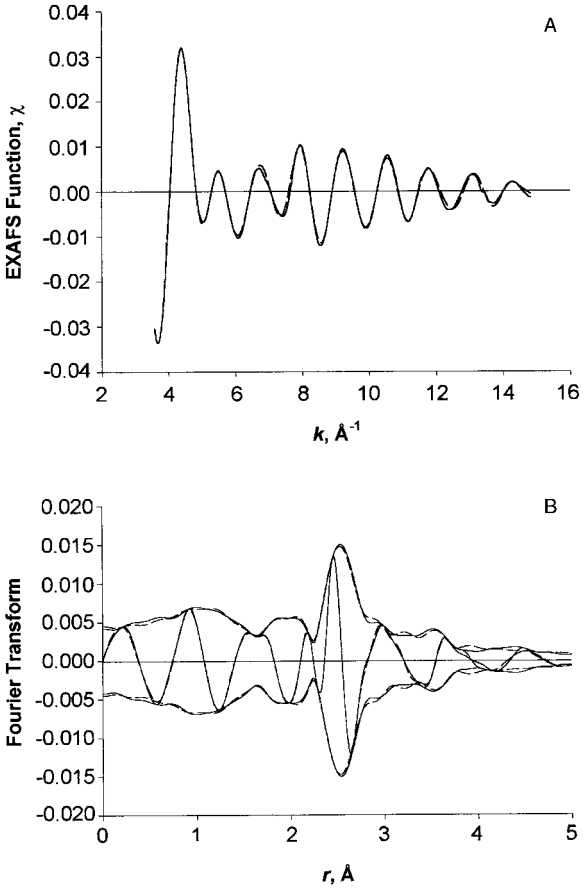

Figure 5. Results of EXAFS analysis characterizing sample initially containing $[Rh(CO)_2(acac)]$ in uncalcined zeolite NaX after treatment in CO at 125 °C and 2 bar for 12 h: A) raw EXAFS function (solid line) and sum of the calculated Rh–Rh + Rh–C_t + Rh–C_{fb} + Rh–O* contributions (dashed line); B) imaginary part and magnitude of Fourier transform (unweighted; $\Delta k = 4.2 - 14.7$ Å^{-1}) of raw EXAFS function (solid line) and sum of the calculated Rh–Rh + Rh–C_t + Rh–C_{fb} + Rh–O* contributions (dashed line) (terms defined in Table 4).

Table 4. X-ray diffraction (XRD) and EXAFS parameters characterizing pure compounds and rhodium clusters formed by CO treatment of zeolite NaX containing $[Rh(CO)_2(acac)]$ at 125 °C and 2 bar.

Sample	Backscatterer	XRD parameters		EXAFS parameters[a]			
		N	R [Å]	N	R [Å]	$\Delta\sigma^2$ [Å^2]	ΔE_0 [eV]
$[NBu_4][Rh_6(CO)_{15}I]$[b]	Rh	4	2.746	–	–	–	–
	C	1.83	1.864	–	–	–	–
	C	2	2.168	–	–	–	–
	O*	3.83	3.061	–	–	–	–
$[NMe_4]_3[Rh_7(CO)_{16}]$[c]	Rh	4.3	2.76	–	–	–	–
	C	1	1.82	–	–	–	–
	C	1.71	1.97	–	–	–	–
	C	1.28	2.14	–	–	–	–
	O*	4	3.06	–	–	–	–
$[Rh(CO)_2(acac)]$ in uncalcined	Rh	–	–	3.66	2.75	−0.00006	3.39
zeolite NaX treated in CO	Na	–	–	0.74	4.00	−0.00834	5.01
at 125 °C and 2 bar for 12 h	C	–	–	2.97	1.88	0.00764	9.87
	C	–	–	3.13	2.10	0.01200	−9.37
	O*	–	–	2.06	2.82	0.00355	25.0
$[Rh(CO)_2(acac)]$ in calcined	Rh	–	–	3.20	2.75	−0.0006	5.72
zeolite NaX treated in CO	Na	–	–	0.46	4.04	−0.00681	5.02
at 125 °C and 2 bar for 12 h	C	–	–	2.94	1.85	0.00614	11.63
	C	–	–	3.21	2.11	0.00607	−8.40
	O*	–	–	2.78	2.82	0.00567	25.0

[a] Notation: N, coordination number for absorber–backscatterer pair; R, absorber–backscatterer distance; $\Delta\sigma^2$, Debye-Waller factor; ΔE_0, inner potential correction. [b] Ref. [47]. [c] Ref. [48].

graphic values for $[Rh_6(CO)_{15}I]^-$ (Table 4). Thus, the EXAFS results support the NMR and infrared data indicating the formation of $[Rh_6(CO)_{15}]^{2-}$ in the zeolite.[49]

The EXAFS data characterizing $[Rh_6(CO)_{15}]^{2-}$ supported in the calcined zeolite (Table 4) indicate that each Rh atom is bonded to about three Rh atoms, on average, at an average distance of 2.76 Å. These results are consistent with the suggestion that $[Rh_6(CO)_{15}]^{2-}$ was present along with lower nuclearity species such as $\{Rh^I(CO)_2\}$. The EXAFS data also indicate Rh–C contributions at 1.88 and 2.10 Å, in approximate agreement with the crystallographic values for $[Rh_6(CO)_{15}I]^-$ (Table 4).

Formation of decarbonylated rhodium clusters and aggregates

Infrared evidence of decarbonylation: Infrared spectra show that the CO ligands were removed from the rhodium clusters when the samples were treated in flowing He at 1 bar as the temperature was ramped from room temperature to 150, 200, 250, or 300 °C at a rate of 3 °C min^{-1} (Figure 6). The treatment

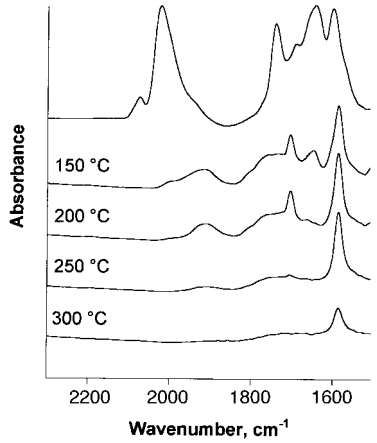

Figure 6. Infrared spectra of $[Rh_6(CO)_{15}]^{2-}$ in uncalcined zeolite NaX and after subsequent treatments in He at the temperatures shown.

at 150 °C led to a spectrum with a broad absorption centered at 1910 cm^{-1} and a shoulder at 1990 cm^{-1}. Treatment of the calcined or uncalcined zeolite-supported rhodium carbonyls in He at 200 or 250 °C for 2 h removed roughly 90 or 99 %, respectively, of the CO ligands (the estimates are based on the ν_{CO} band intensities). Decarbonylation was complete at 300 °C (Figure 6).

Alternatively, the zeolites containing rhodium carbonyl clusters were treated in flowing H_2 at 1 bar as the temperature was ramped in the same way. This treatment led to the disappearance of the terminal $\tilde{\nu}_{CO}$ bands at 2074w, 2022vs, and 1995 cm^{-1} sh, characteristic of the uncalcined sample, and to the disappearance of the terminal $\tilde{\nu}_{CO}$ bands at 2100w, 2050sh, 2015s, and 1990 cm^{-1} sh, characteristic of the calcined sample (Figure 7). The peak at 1745 cm^{-1}, indicating face-bridging CO ligands, disappeared from the spectra of both the calcined and uncalcined samples. Furthermore, a broad new $\tilde{\nu}_{CO}$ peak appeared, centered in the range from about 1935 cm^{-1} at 150 °C to about 1890 cm^{-1} at 300 °C, at which temperature the decarbonylation was nearly complete (Figure 7). Treatment of the calcined or uncalcined zeolite-supported rhodium carbonyls in H_2 at 200, 250, or 300 °C for 2 h removed roughly 70, 85, or 95 %, respectively, of the CO ligands (the estimates are based on the $\tilde{\nu}_{CO}$ band intensities).

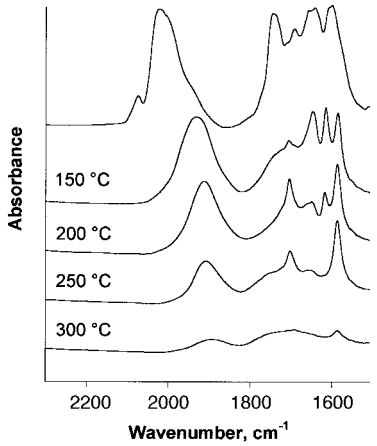

Figure 7. Infrared spectrum of $[Rh_6(CO)_{15}]^{2-}$ in uncalcined zeolite NaX and spectra of sample following treatments in H_2 at the temperatures shown.

EXAFS evidence of decarbonylated rhodium clusters and aggregates: EXAFS spectra of the decarbonylated rhodium (formed by the treatment of the zeolite-supported rhodium carbonyls in He or in H_2 at 200, 250, or 300 °C for 2 h) show oscillations up to values of k equal to about 16 Å^{-1}, consistent with Rh–Rh bonds and clusters (Figure 8). The data characterizing the clusters formed by decarbonylation in He at 200 °C could be fitted satisfactorily only when the following contributions were included: Rh–Rh (at about 2.69 Å), Rh–O (2.1 Å), a small Rh–C (1.95 Å), and a small (tentatively assigned) Rh–Na (3.85 Å) (Table 5, samples 1 and 3). There was no significant change in the Rh–Rh coordination number as a result of cluster decarbonylation in He at successively higher temperatures up to 300 °C (Table 5, Figure 8).

The data characterizing the samples treated in H_2 (samples 6–10, Table 6) also indicate the presence of a Rh–Rh contribution (2.68 Å) as well as contributions that can be attributed to Rh–O, Rh–C, and Rh–O* (O* is carbonyl oxygen), with distances of 2.11, 1.97, and 3.0 Å, respectively. In contrast to the decarbonylation of the encaged rhodium clusters in He, the decarbonylation in H_2 at temperatures >200 °C was accompanied by an increase in the Rh–Rh coordination number (Table 6, Figure 9), indicating aggregation of the rhodium.[50] These results demonstrate the presence of clusters with sizes ranging from six or fewer metal atoms (Rh–Rh first-shell coordination number ≤ 4) to as many as about 40 atoms, on average (Rh–Rh first-shell coordination number = 7; Table 6);[52] aggregation evidently occurred as a result of treatment in H_2 at the higher temperatures (we now refer to aggregates in order to differentiate them from the clusters that (nearly) retained the nuclearities of the precursor $[Rh_6(CO)_{15}]^{2-}$). The aggregates were no doubt present in part outside the zeolite cages and on external surfaces of the zeolite crystallites. A comparison of the X-ray absorption near-edge spectrum of the clusters formed in He at 300 °C with that of the aggregates formed in

  0947-6539/99/0510-2904 $ 17.50+.50/0 Chem. Eur. J. 1999, 5, No. 10

Table 5. EXAFS results characterizing rhodium clusters supported on zeolite NaX[a] formed by decarbonylation of $[Rh_6(CO)_{15}]^{2-}$ in He.

Sample no.	Support preparation conditions[b]			Conditions of treatment of sample containing $[Rh_6(CO)_{15}]^{2-}$			Back-scatterer	EXAFS parameters[c]				Approximate cluster nuclearity[d]
	treatment gas	T [°C]	t [h]	treatment gas	T [°C]	t [h]		N	R [Å]	$\Delta\sigma^2$ [Å^2]	ΔE_0 [eV]	
1	–	25	–	He	200	2	Rh	2.6	2.65	0.00384	12.6	6
							O	1.0	2.25	0.01500	−20.0	
							C	0.9	1.97	0.00501	−14.1	
	–	25	–	He	250	2	Rh	–	–	–	–	
							O	–	–	–	–	
							C	–	–	–	–	
2	–	25	–	He	300	2	Rh	2.6	2.65	0.00423	7.2	6
							O	1.1	2.19	0.01500	−15.4	
							C	0.4	1.96	−0.00410	−18.5	
3	O_2	300	4	He	200	2	Rh	2.8	2.69	0.00355	7.9	6
							O	1.3	2.15	0.01500	−10.0	
							C	1.2	1.94	0.00700	−9.1	
4	O_2	300	4	He	250	2	Rh	2.5	2.67	0.00456	7.7	6
							O	1.2	2.17	0.01500	−18.0	
							C	0.7	1.96	−0.00149	−18.5	
5	O_2	300	4	He	300	2	Rh	2.6	2.66	0.00432	3.6	6
							O	1.4	2.12	0.01500	−14.4	
							C	0.7	1.96	−0.00196	−25.0	

[a] Notation: terms defined in Table 4; T = temperature, t = time. [b] All samples were evacuated at treatment temperature for 12 h (following gas treatment for samples treated in O_2). [c] Data for all samples were fitted for a Rh–Na contribution at about 4 Å (typical values: $N = 0.5$, $\Delta\sigma^2 = 0.01$ Å^2, $\Delta E_0 = 3$ eV). [d] values are only approximate; see text.

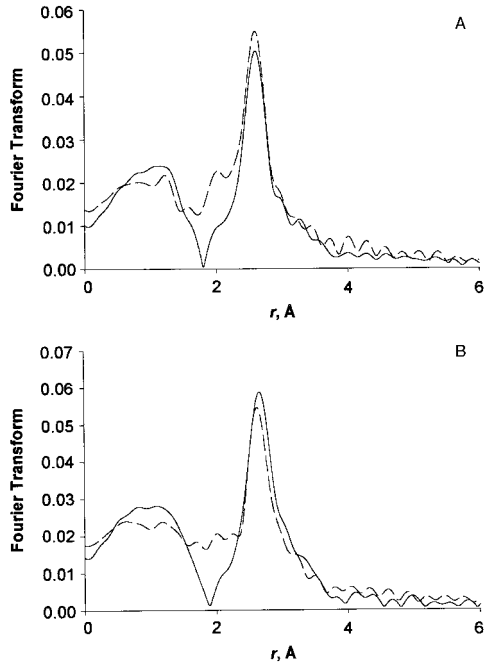

Figure 8. A) Fourier transforms of the raw EXAFS data characterizing calcined zeolite NaX-supported rhodium clusters formed by the decarbonylation of $[Rh_6(CO)_{15}]^{2-}$ at 200 °C (solid line) or 300 °C (dashed line) in the presence of He. B) Fourier transforms of the raw EXAFS data characterizing uncalcined zeolite NaX-supported rhodium clusters formed by the decarbonylation of $[Rh_6(CO)_{15}]^{2-}$ at 200 °C (solid line) or 300 °C (dashed line) in the presence of He.

H_2 at 300 °C shows a higher edge intensity, which characterizes the latter (Figure 10); the clusters may be electron deficient relative to the aggregates.[53]

Recarbonylation of decarbonylated rhodium clusters: With CO at 1 bar flowing through the infrared cell containing the decarbonylated clusters in the uncalcined zeolite, the temperature was ramped from room temperature to 125 °C and held for 12 h. The infrared spectrum (not shown) indicates that the sample that had been decarbonylated in the presence of He was not reconverted into $[Rh_6(CO)_{15}]^{2-}$, but was instead converted into a mixture of rhodium carbonyls with $\tilde{\nu}_{CO}$ bands at 2094m, 2013s, 1833w, and 1749m cm^{-1}. The color of the recarbonylated sample was light brown, whereas that of the sample prior to decarbonylation was green.

In contrast, the uncalcined sample treated in H_2 at 200 °C, from which about 70 % of the CO ligands had been removed, was characterized after recarbonylation by a spectrum (not shown) nearly identical to that of the sample prior to decarbonylation; this demonstrates that the partial decarbonylation in the presence of H_2 was reversible. Consistent with this conclusion, the color of the sample again became green.

Oxidative fragmentation and reconstruction of rhodium carbonyls: When the sample containing predominantly $[Rh_6(CO)_{15}]^{2-}$ in the zeolite was exposed to air at room temperature, the color changed almost instantaneously from green to light yellowish brown, and the infrared spectrum included terminal $\tilde{\nu}_{CO}$ bands at 2089 and 2010 cm^{-1}, indicative of mononuclear rhodium dicarbonyls.[25–28] After CO at 1 bar flowed over this oxidized sample at 125 °C for 12 h, the spectrum of the original rhodium carbonyl reappeared, indicating that $[Rh_6(CO)_{15}]^{2-}$ had been reconstructed and the oxidative fragmentation reversed.[54]

Toluene hydrogenation catalyzed by decarbonylated rhodium clusters and aggregates

Zeolite-supported rhodium clusters: When a tubular flow reactor was packed with only inert α-Al_2O_3 particles, no conversion of toluene and H_2 at 100 °C and 1 bar was

Table 6. EXAFS results characterizing rhodium clusters supported on zeolite NaX[a] formed by decarbonylation of $[Rh_6(CO)_{15}]^{2-}$ in H_2.

Sample no.	Support preparation conditions[b]			Conditions of treatment of sample containing $[Rh_6(CO)_{16}]$			Back-scatterer	EXAFS parameters[c]				Approximate cluster nuclearity[d]
	treatment gas	T [°C]	t [h]	treatment gas	T [°C]	t [h]		N	R [Å]	$\Delta\sigma^2$ [Å^2]	ΔE_0 [eV]	
6	–	25	–	H_2	200	2	Rh	3.6	2.69	0.00643	12.7	6
							O	1.5	2.29	0.01290	−20.0	
							C	3.8	1.99	0.01277	−9.4	
	–	25	–	H_2	250	2	Rh	–	–	–	–	
							O	–	–	–	–	
							C	–	–	–	–	
7	–	25	–	H_2	300	2	Rh	6.2	2.65	0.00422	5.0	20–30
							O	0.6	2.30	0.01244	−18.4	
							C	–	–	–	–	
8	O_2	300	4	H_2	200	2	Rh	3.8	2.71	0.00686	11.1	6
							O	1.4	2.27	0.01244	−19.3	
							C	3.0	2.00	0.01137	−9.1	
9	O_2	300	4	H_2	250	2	Rh	4.9	2.67	0.00456	7.7	6–10
							O	0.7	2.11	0.00484	−12.0	
							C	0.9	1.95	0.00171	−10.8	
10	O_2	300	4	H_2	300	2	Rh	7.0	2.66	0.00345	2.0	30–40
							O	–	2.10	–	–	
							C	–	–	–	–	

[a] Notation: terms defined in Table 5. [b] All samples were evacuated at treatment temperature for 12 h (following gas treatment for samples treated in O_2). [c] Data for all samples were fitted for a Rh–Na contribution at about 4 Å (typical values: $N = 0.7$, $\Delta\sigma^2 = 0.03$ Å^2, $\Delta E_0 = 3$ eV). [d] Values only approximate; see text.

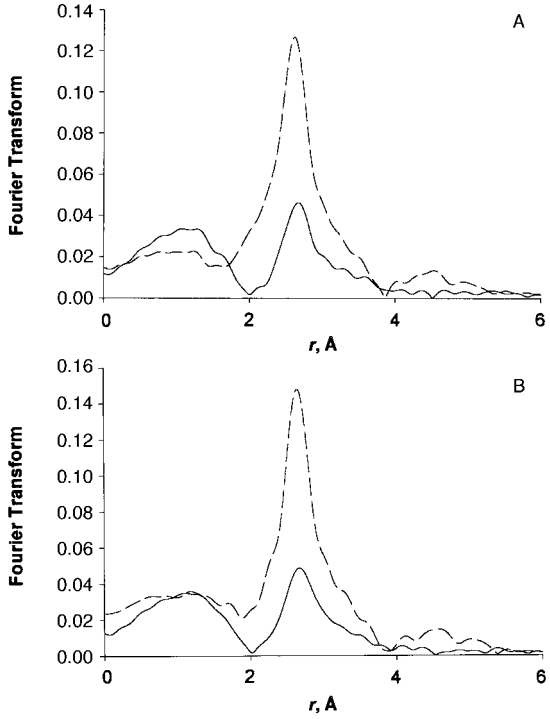

Figure 9. A) Fourier transforms of the raw EXAFS data characterizing calcined zeolite NaX-supported rhodium clusters formed by the decarbonylation of $[Rh_6(CO)_{15}]^{2-}$ at 200 °C (solid line) or 300 °C (dashed line) in the presence of H_2. B) Fourier transforms of the raw EXAFS data characterizing uncalcined zeolite NaX-supported rhodium clusters formed by the decarbonylation of $[Rh_6(CO)_{15}]^{2-}$ at 200 °C (solid line) or 300 °C (dashed line) in the presence of H_2.

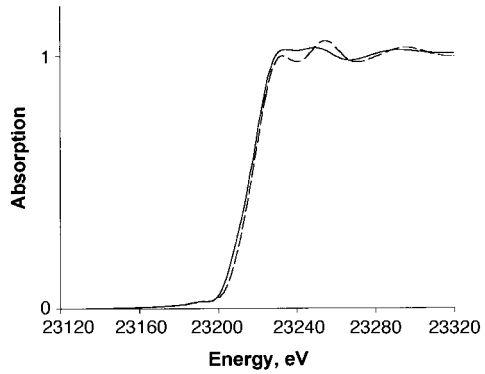

Figure 10. X-ray absorption near-edge spectra characterizing zeolite NaX-supported sample formed by treatment of $[Rh_6(CO)_{15}]^{2-}$ in He (giving clusters, dashed line) or in H_2 (giving aggregates, solid line) at 300 °C.

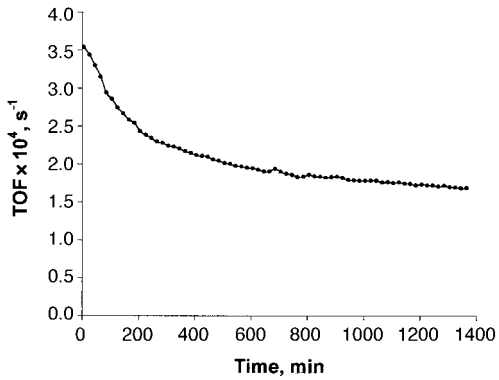

Figure 11. Catalytic activity of rhodium clusters formed by treatment of zeolite NaX-supported $[Rh_6(CO)_{15}]^{2-}$ in He at 300 °C for toluene hydrogenation at 80 °C as a function of time on stream in a flow reactor.

observed, but when this mixture passed through the reactor containing the decarbonylated rhodium clusters (samples 2, 4, and 5, Table 5), methylcyclohexane, the catalytic reaction product, was observed.

Following an induction period of about 2 h (Figure 11), each catalyst underwent a steady, slow deactivation over a period of about four days, after which it had lost about 90 % of its activity.[57] The reported rates were found by extrapolating the data to zero time on stream (excluding the induction period; e.g., Figure 11). The rates were determined from

0947-6539/99/0510-2906 $ 17.50+.50/0 *Chem. Eur. J.* **1999**, *5*, No. 10

differential conversions (< 0.5 %), and they are represented as turnover frequencies in units of [molecules of toluene converted (Rh atom)$^{-1}$ s^{-1}] (Table 7).[58] Details of the catalysis experiments are given elsewhere, with a performance comparison of these and similar catalysts.[59]

Zeolite-supported rhodium aggregates: Toluene hydrogenation experiments were done as stated above with the catalysts consisting of aggregates of rhodium supported on zeolite NaX (samples 7, 9, and 10, Table 6). The aggregated rhodium catalysts are characterized by toluene hydrogenation activities greater than that of the unaggregated supported clusters (samples 1–5, 6, and 8, Tables 5 and 6). The values in Table 7 are reported per total Rh atom; those rates characterizing the aggregated rhodium are not quite equal to turnover frequencies because not all the Rh atoms were surface atoms, as shown by the EXAFS results (Tables 5 and 6). This comparison of the activities of the clusters and aggregates consequently understates the difference in their intrinsic activities.[60] Estimates of turnover frequencies, calculated from the reaction rates and cluster nuclearities estimated from Rh–Rh coordination numbers (Table 7), show that the aggregated rhodium (samples 7, 9, and 10) is characterized by turnover frequencies an order of magnitude greater than those of the decarbonylated clusters (samples 2, 4, and 5).

Discussion

Analogy between rhodium carbonyl cluster synthesis in zeolite cages and that in solution: The reactions of rhodium carbonyls in neutral or slightly acidic solutions typically give neutral products, often clusters. For example, $[Rh(CO)_2Cl]_2$ reacts with CO and water in aqueous methanol to give $[Rh_4(CO)_{12}]$ and $[Rh_6(CO)_{16}]$ [Eqs. (1) and (2)].[61] Analogous chemistry is illustrated by the formation of $[Rh_4(CO)_{12}]$ and $[Rh_6(CO)_{16}]$ in zeolite NaY;[30, 62] water or surface hydroxyl groups facilitate this intracage chemistry.[30]

$$2[Rh_2(CO)_4Cl_2] + 6CO + 2H_2O \longrightarrow [Rh_4(CO)_{12}] + 2CO_2 + 4HCl \quad (1)$$

$$[Rh_2(CO)_4Cl_2] + 7CO + 3H_2O \longrightarrow [Rh_6(CO)_{16}] + 3CO_2 + 6HCl \quad (2)$$

Rhodium carbonyl anions are formed in solution by nucleophilic attack on neutral clusters. $[Rh_6(CO)_{15}X]^-$ (X = Cl, Br, I, CN, SCN) is formed from $[Rh_6(CO)_{16}]$ by reaction with halides or pseudohalides. Carboalkoxy and carboamido anions (X = COOMe, COOEt, and CONH*i*Pr) are formed by nucleophilic attack of alcohols on $[Rh_6(CO)_{16}]$ in the presence of Na_2CO_3 or by nucleophilic attack of amines, as represented by Equation (3), in which M is an alkali metal.[63] The rhodium carbonyl is reduced further, giving anionic clusters, when the solution is more strongly basic or reducing. Equations (4) and (5) illustrate the step-by-step reduction.[63] Reductive carbonylation of $[Rh_2(CO)_2Cl_2]$ in a strongly basic solution may also result in the formation of $[Rh_{12}(CO)_{30}]^{2-}$,[64] $[Rh_5(CO)_{15}]^-$,[15] $[Rh_6(CO)_{15}]^{2-}$,[65] $[Rh_7(CO)_{16}]^{3-}$,[65] or $[Rh_4(CO)_{11}]^{2-}$.[66]

$$[Rh_6(CO)_{16}] + MX \longrightarrow M[Rh_6(CO)_{15}X] + CO \quad (3)$$

$$6[Rh_2(CO)_4Cl_2] + 7Na_2CO_3 + 2ROH \longrightarrow 2Na[Rh_6(CO)_{15}(COOR)] + 4CO + CO_2 + H_2O \quad (4)$$

$$Na[Rh_6(CO)_{15}(COOR)] + 2NaOH \longrightarrow Na_2[Rh_6(CO)_{15}] + NaHCO_3 + ROH \quad (5)$$

Extending the analogy between solution chemistry and intracage chemistry of rhodium carbonyls illustrated by the formation of $[Rh_6(CO)_{16}]$ in neutral solutions and in zeolite NaY,[30] we expect similar chemistry leading to anion formation to occur on basic surfaces and in basic zeolites such as NaX.[38] Examples of rhodium carbonyl clusters that form on basic surfaces are $[Rh_{12}(CO)_{30}]^{2-}$,[67] $[Rh_5(CO)_{15}]^-$,[67] and $[Rh_6(CO)_{15}]^{2-}$ on MgO.[68, 69] Similarly, $[Ir_6(CO)_{15}]^{2-}$ was synthesized from $[Ir(CO)_2(acac)]$ in zeolite NaX[38] and $[Ru_6(CO)_{18}]^{2-}$ from a salt precursor in this zeolite, as in basic solutions.[70] These results indicate that the formation of $[Rh_6(CO)_{15}]^{2-}$ in zeolite NaX is related to the zeolite basicity.

Intracage chemistry of $[Rh_6(CO)_{15}]^{2-}$: X-ray crystallographic data[47] show that the diameter of $[Rh_6(CO)_{15}]^{2-}$ is about 10 Å; consequently, this cluster fits in the supercages of zeolite NaX, which have diameters of about 11.5 Å,[71] but it is too large to fit through the windows connecting these cages, which have

Table 7. Toluene hydrogenation catalyzed by zeolite NaX-supported rhodium clusters and aggregates.[a]

Sample no.[b]	Degree of decarbonyalation	N_{Rh-Rh}	Approximate cluster nuclearity[d]	T [°C]	(Rate × 10^8)[e] [mol g^{-1} s^{-1}]	(TOF × 10^4)[f] [s^{-1}]	Apparent activation energy [kcal mol^{-1}]
1	nearly complete	2.6	≤ 6	80	6.6	3.0	10.4
				100	19	9.0	
				120	28	13	
2	complete	2.6	≤ 6	80	6.6	3.0	11.6
				100	19	9.0	
				120	34	16	
3	nearly complete	2.8	≤ 6	100	17	8.0	–
4	complete	2.5	≤ 6	100	15	7.0	–
5	complete	2.6	≤ 6	100	13	6.0	–
7	nearly complete	6.2	20–30	100	154	70	–
10	nearly complete	7.0	30–40	100	220	100	–

[a] Notation as in Table 4. [b] Sample preparations as defined in Tables 5 and 6. [c] All samples are evacuated at treatment temperature for 12 h (following gas treatment for samples treated in O_2). [d] Ref. [52]. [e] rate = (moles of toluene converted)/[(g of catalyst) × s]. [f] TOF = (moles of toluene converted)/[(moles of rhodium) × s].

diameters of about 7.5 Å.[71] No more than one of these clusters would fit in a single supercage, and so we infer that the clusters were isolated and formed by a ship-in-a-bottle synthesis. If all the rhodium were converted to $[Rh_6(CO)_{15}]^{2-}$, then about one in 15 supercages would contain a cluster. We infer that each cluster was built up from intermediates that were mononuclear rhodium complexes, as in the solution synthesis; the mononuclear intermediates were evidently mobile in the zeolite pores. The evidence that some of the rhodium was present as mononuclear rhodium subcarbonyls indicates that there were competing reactions of the intermediates formed from $[Rh(CO)_2(acac)]$.

Only with ^{13}C NMR spectroscopy were we able to determine that $[Rh_6(CO)_{15}]^{2-}$ formed in zeolite NaX. In contrast, $[Rh_6(CO)_{16}]$ in zeolite NaY could be identified from just infrared and EXAFS data.[30] The NMR data provide some of the first evidence of yields of organometallic reactions in cages; we expect NMR spectroscopy to become much more important in the development of intracage chemistry.

The structure of $[Rh_6(CO)_{15}]^{2-}$ in the zeolite is evidently similar to that in solution, as shown by the infrared and NMR spectra. However, there are some differences associated with the cage walls, on the one hand, versus the solvent on the other. The cations balancing the charge of the cluster anions in the cages are still not fully known; the carbonyl anions are expected to interact with the Na^+ exchange ions needed for charge neutrality in the original zeolite,[72] and there could be interactions of the anions with OH groups formed from water initially present in the zeolite or from the acac ligands.

The ^{13}C NMR spectrum of $[Rh_6(CO)_{15}]^{2-}$ in solution consists of a single septet centered at $\delta = 209$, indicating that all the CO ligands are equivalent.[6] However, X-ray diffraction data show that $[Rh_6(CO)_{16}]$ in the solid state has two types of CO ligands.[47] In the solid state, $[Rh_6(CO)_{15}]^{2-}$, without a face-bridging CO ligand, is coordinated rigidly through the face to a cation. When the cluster is in solution, the cation is mobile enough to expose edges of the face. Because the Rh atoms of the face are then coordinatively unsaturated, edge-bridging CO ligands form, and there is rapid CO intraexchange.[73] Therefore, on the NMR timescale only one peak is observed. Because CO ligands may rapidly undergo intraexchange over the metal framework of $[Rh_6(CO)_{15}]^{2-}$, ^{13}C NMR spectra provide information about the interaction of the cluster with the zeolite walls. Like the ^{13}C NMR spectrum of $[Rh_6(CO)_{15}]^{2-}$ in solution, that of the cluster in zeolite NaX at 80 °C indicates that all the CO ligands undergo rapid exchange over the metal frame; this implies a lack of strong interactions between the cluster and the zeolite walls. However, the three peaks in the room-temperature spectrum indicate that the intraexchange of CO ligands is slower than at 80 °C and that there are three distinct types of CO ligands, which are likely to be terminal CO and two types of bridging CO; the cluster now acts more like that found in the solid state. These results indicate that the low-temperature interactions between the cluster and the zeolite are relatively strong, with a Na^+ ion possibly being coordinated to the otherwise coordinatively unsaturated cluster face, hindering CO intraexchange. If the exchange were slow on the NMR timescale, then we might expect to observe peaks for terminal CO ligands, edge-bridging CO ligands on the unsaturated face, and face-bridging CO ligands.

The infrared spectra give further evidence of the interaction of the cluster anions with the cage walls, as follows: there was a shift of the terminal-carbonyl-stretching frequencies characterizing the supported clusters to higher wavenumbers and a shift in the bridging carbonyl-stretching frequencies to lower wavenumbers relative to those of the cluster in solution. These shifts indicate interactions of CO with zeolite Lewis acid sites,[74] for example, Na^+. Support for this interpretation is provided by similar shifts observed for iridium and rhodium clusters in zeolites (Table 8).

Table 8. Comparison of infrared spectra characterizing iridium and rhodium carbonyl clusters in solution and on supports.

Cluster	Solvent [ref.]	Color[a]	Zeolite support [ref.]	ΔT[b] [cm^{-1}]	ΔB[c] [cm^{-1}]
$[Ir_4(CO)_{12}]$	THF [33]	–	NaY [34]	4	–
$[Ir_6(CO)_{16}]$	CH_2Cl_2, [35]	–	NaY [35,36]	21	– 53
$[Rh_4(CO)_{12}]$	$CHCl_3$ [61]	–	NaY [31,32]	7	– 41
$[Rh_6(CO)_{16}]$	$CHCl_3$ [61,62]	–	NaY [30 – 32]	23	– 40
$[Ir_4(CO)_{11}]^-$	THF [37]	–	NaX [38]	18	– 69
$[Ir_6(CO)_{15}]^{2-}$	THF [35]	–	NaX [38]	29	– 65
$[Rh_4(CO)_{11}]^{2-}$	THF [40]	red	NaX[d]	12	– 97
$[Rh_5(CO)_{15}]^-$	THF [41]	red	NaX[d]	12	– 100
$[Rh_6(CO)_{15}]^{2-}$	CH_3CN [42]	green	NaX[d]	32	– 18
$[Rh_7(CO)_{16}]^{3-}$	CH_3CN [42]	dark green	NaX[d]	67	– 28

[a] The color pertains to the color of the carbonyl cluster in the solvent listed. [b] ΔT is the value of the main terminal peak position characterizing the supported metal carbonyl cluster minus the value of the main terminal peak position characterizing the same cluster in solution. [c] ΔB is the value of the main bridging peak position characterizing the supported metal carbonyl cluster minus the value of the main bridging peak position characterizing the same cluster in solution. [d] This pertains to the sample formed by flowing CO over $[Rh(CO)_2(acac)]$-containing zeolite NaX at 125 °C. The sample was green in color.

The strongest terminal-carbonyl band of $[Rh_6(CO)_{15}]^{2-}$ in zeolite NaX is shifted 32 cm^{-1} to higher wavenumber (Table 8). The average shift of the principal terminal-carbonyl band of rhodium or iridium carbonyls in zeolites NaY and NaX (Table 8) is about 17 cm^{-1}. The relatively large shift observed for the terminal-carbonyl band of $[Rh_6(CO)_{15}]^{2-}$ in zeolite NaX indicates a relatively strong interaction with the zeolite through its CO ligands.

To summarize, the NMR data indicate the formation of $[Rh_6(CO)_{15}]^{2-}$ in the zeolite, and the results are supported by the infrared and EXAFS data; the dimensions of the cluster and the zeolite cages and windows indicate that the cluster synthesis was a ship-in-a-bottle synthesis. The chemistry is analogous to that in basic solutions. The NMR and infrared spectroscopic results indicate that, at room temperature, cluster – zeolite interactions are strong and CO intraexchange negligible, whereas at 80 °C these interactions are weak, allowing rapid intraexchange of CO ligands on the metal frame.

Quasimolecular rhodium clusters formed by decarbonylation of $[Rh_6(CO)_{15}]^{2-}$: Clusters that were partially decarbonylated [as shown by CO band intensities (Figure 7)], formed by

0947-6539/99/0510-2908 $ 17.50+.50/0 *Chem. Eur. J.* **1999**, *5*, No. 10

treatment of $[Rh_6(CO)_{15}]^{2-}$ in the uncalcined zeolite in H_2 at 200 °C (sample 6, Table 6), evidently had a structure similar to that of $[Rh_6(CO)_{15}]^{2-}$, but with fewer CO ligands and possibly with hydride ligands replacing CO ligands. The Rh–Rh coordination number (3.6), characteristic of the partially decarbonylated rhodium species in the uncalcined zeolite (sample 6, Table 6), is essentially the same as that of the precursor $[Rh_6(CO)_{15}]^{2-}$ (3.7). Similarly, the Rh–Rh coordination number (3.6), characteristic of the partially decarbonylated clusters (sample 8, Table 6) formed from $[Rh_6(CO)_{15}]^{2-}$ in calcined zeolite NaX, is indistinguishable, within the expected experimental uncertainty (±15–20%), from that of the precursor rhodium carbonyl cluster (3.2) [present with rhodium subcarbonyls]. These results suggest that the partially decarbonylated clusters (samples 6 and 8, Table 6) had the same octahedral metal frame as the precursor $[Rh_6(CO)_{15}]^{2-}$. The EXAFS data also provide evidence of CO ligands in these clusters, that is, a Rh–C contribution at 1.97 Å and a Rh–O* contribution (with multiple scattering) at about 3 Å.

Treatment of the supported metal carbonyl clusters in He led to nearly complete decarbonylation after 2 h at 200 °C (samples 1 and 3), as shown by the infrared spectra (Figure 6); the same result was obtained whether or not the zeolite had been calcined. The Rh–Rh coordination numbers characterizing these decarbonylated clusters ranged from 2.5 to 2.8 (samples 1–5, Table 5). These values are significantly smaller than the coordination number characterizing $[Rh_6(CO)_{15}]^{2-}$ and the partially decarbonylated clusters (Table 6, samples 6 and 8). If it can be assumed that the cluster nuclearities were retained during decarbonylation, then the results suggest that the frames were no longer octahedral, but flattened (raftlike), presumably as a consequence of their interactions with the cage walls.[77] Alternatively, the clusters might have been smaller than six-metal-atom clusters, on average; the possibility of some oxidative fragmentation (with surface OH groups being reactants) to give some mononuclear fragments is not ruled out.[78]

To summarize, virtually molecular clusters of rhodium, containing, on average, about six Rh atoms, CO ligands, and (we suggest) H ligands, formed in zeolite cages as a result of the partial decarbonylation of $[Rh_6(CO)_{15}]^{2-}$ in H_2 at 200 °C (samples 6 and 8, Table 6). When the clusters were fully decarbonylated by treatment in He, flattened or fragmented clusters formed (samples 1–5, Table 5).

Formation of aggregated rhodium: When either the calcined or uncalcined zeolite containing $[Rh_6(CO)_{15}]^{2-}$ was treated in H_2 at temperatures >200 °C, rhodium aggregates formed (samples 7, 9, and 10, Table 6). The decarbonylation at 250 °C led to a Rh–Rh coordination number of about 5 (sample 9, Table 6), indicating an average cluster nuclearity of about 10–12 atoms.[52] Subsequent treatment at 300 °C resulted in a coordination number of about 7, consistent with aggregates having an average of about 40 atoms each.[52] Although some of the aggregates might fit in the cages, it is likely that metal migrated outside of the zeolite cages or caused cages to burst.[79, 80] These results imply migration of rhodium through the zeolite channels; partially decarbonylated clusters were possibly transported intact, as they could be small enough to fit through the windows (with diameters of about 7.5 Å).

Recarbonylation of rhodium clusters and reversible oxidative fragmentation of $[Rh_6(CO)_{15}]^{2-}$ and subsequent reductive carbonylation: When CO was introduced into the zeolite sample containing the fully decarbonylated clusters, $[Rh_6(CO)_{15}]^{2-}$ was not reformed. Instead, rhodium subcarbonyls, $\{Rh(CO)_2\}$, formed, as indicated by the infrared bands at 2094 and 2013 cm^{-1}. Along with these terminal CO bands, absorptions at 1835 and 1749 cm^{-1} were observed, indicating both edge- and face-bridging CO groups. These results imply that mixtures formed, which included clusters, and that the decarbonylation of the original clusters in He was not reversible under these conditions. In contrast, the partially decarbonylated clusters treated in H_2 at 200 °C (and presumably incorporating hydride ligands), upon exposure to CO at 125 °C, gave a spectrum nearly matching that of $[Rh_6(CO)_{15}]^{2-}$, indicating the reversibility of the partial decarbonylation in H_2.

Air oxidation of $[Rh_6(CO)_{15}]^{2-}$ in uncalcined zeolite NaX led to the formation of $\{Rh(CO)_2\}$, with no clusters remaining. Such rhodium subcarbonyls have been postulated to have two oxygen ligands (part of the zeolite wall) and two terminally bonded CO ligands; water is also a possible ligand.[25–28] Subsequent treatment in CO at 1 bar and 125 °C for 12 h led to reconstruction of $[Rh_6(CO)_{15}]^{2-}$, the product of reductive carbonylation. The reversible reactions are inferred to take place within the zeolite cages,[81] although some migration of rhodium carbonyls between cages is not excluded.[55] The reversible formation of $[Rh_6(CO)_{15}]^{2-}$ took place even though the decarbonylation product clearly did not retain the octahedral metal frame.

Toluene hydrogenation catalyzed by supported rhodium clusters: Toluene hydrogenation,[82] like alkene hydrogenations, is regarded as a structure-insensitive catalytic reaction, taking place with turnover frequencies that are almost independent of the metal cluster or particle size. However, only few data exist for metal cluster catalysts smaller than about 20 Å in average diameter.[83] The results show that the decarbonylated zeolite-supported clusters consisting of only about six metal atoms each, on average, are, like metallic rhodium, active catalysts for toluene hydrogenation. However, they are less active than the larger aggregates of rhodium on the zeolite support (Table 8). This result is consistent with the strong dependence of catalytic activity for toluene hydrogenation on cluster or aggregate size demonstrated for iridium supported on γ-Al_2O_3.[84] The reasons for the cluster size dependence of the catalytic activity are debated and discussed elsewhere.[84]

Conclusion

$[Rh_6(CO)_{15}]^{2-}$ was synthesized in the supercages of zeolite NaX by carbonylation of $[Rh(CO)_2(acac)]$ and characterized by ^{13}C NMR, infrared, and EXAFS spectroscopies. Synthesis with an uncalcined zeolite gave a higher yield of

$[Rh_6(CO)_{15}]^{2-}$ (about 83%) than that with a calcined zeolite; this suggests a role of water or surface hydroxyl groups. The supported rhodium carbonyls were treated in He or H_2 at 200, 250, or 300 °C to remove carbonyl ligands. When partial decarbonylation took place in the presence of H_2 at 200 °C, new rhodium carbonyl clusters formed, evidently with the same metal frame as the precursor $[Rh_6(CO)_{15}]^{2-}$. The clusters that had been partially decarbonylated in H_2 or oxidatively fragmented by treatment in air to give rhodium subcarbonyls could be carbonylated to reform $[Rh_6(CO)_{15}]^{2-}$ in the zeolite. Decarbonylation in H_2 at 250 and at 300 °C resulted in the aggregation of the rhodium, but decarbonylation in He gave small rhodium clusters; these were fully decarbonylated and raftlike or possibly partially fragmented. The rhodium clusters formed by the intracage decarbonylation of $[Rh_6(CO)_{15}]^{2-}$ catalyze the hydrogenation of toluene; the data show a strong dependence of catalytic activity on cluster or aggregate size.

Experimental Section

Materials and sample preparation: All syntheses and sample transfers were conducted with exclusion of air and moisture on a double-manifold Schlenk vacuum line and in a N_2-filled Vacuum Atmospheres drybox. N_2 and He (99.999%) were passed through traps containing particles of supported Cu and zeolite to remove traces of O_2 and moisture. CO (Puritan Bennett, UHP grade) was passed through similar traps. Pentanes (Fisher, HPLC grade) were dried over sodium/benzophenone and deoxygenated by sparging with N_2 for 2 h. Tetrahydrofuran (THF) (Fisher, HPLC grade) was dried over sodium/benzophenone and similarly deoxygenated. $CHCl_3$ (Fisher, HPLC grade), $[Rh(CO)_2(acac)]$ (Strem, 99%), [PPN]Cl (Aldrich), and Rh_2O_3 (anhydrous) (Strem, 99.9%) were used as received. Zeolite NaX (Si/Al = 1.4, Davison Division, W. R. Grace and Co.) was either evacuated for 12 h or calcined in O_2 for 4 h at 300 °C and then evacuated at 300 °C for 12 h. Following the treatment, the zeolite powder support was brought in contact with an amount of a solution of $[Rh(CO)_2(acac)]$ to give a sample containing 2.25 wt% Rh after removal of the solvent.[85] In each preparation, the support was brought in contact with the precursor by slurrying in dried pentanes in a Schlenk flask under N_2. After stirring of the slurry at room temperature for several days, the solvent was removed by evacuation and the solid dried in vacuo (pressure $< 10^{-3}$ Torr) overnight. The resulting solids were stored in the drybox. Samples were carbonylated in a flow reactor with CO at 2 bar (or 1 bar when the reactor was an infrared cell) and were decarbonylated in an EXAFS cell at 1 bar in the presence of flowing H_2 or He.

Infrared spectroscopy: Transmission infrared spectra of the samples were collected with a Bruker IFS-66V spectrometer with a spectral resolution of 0.1 cm^{-1}. Samples of the supported precursors and those prepared by carbonylation were pressed into thin self-supporting wafers in the drybox and loaded into a controlled-atmosphere infrared cell. The cell was incorporated in a flow system, through which purified He, H_2, or CO could be passed.

Attempted extraction of metal carbonyls from zeolite NaX: Attempts were made to extract rhodium carbonyls from the zeolite by letting samples come into contact with freshly distilled THF, with or without [PPN][Cl], under N_2. The supernatant liquid was transferred by syringe into a solution infrared cell and quickly scanned to test for metal carbonyls.

EXAFS data collection: The EXAFS experiments were performed on beamline 2-3 of the Stanford Synchrotron Radiation Laboratory (SSRL) at the Stanford Linear Accelerator Center, Stanford, CA, and on X-ray beamline X-11A at the National Synchrotron Light Source (NSLS) at Brookhaven National laboratory, Upton, NY. The storage ring at SSRL operated at an energy of 3 GeV and that at NSLS 2.5 GeV; the beam current was between 70 and 100 mA at SSRL and between 140 and 240 mA at NSLS. Details of the experiments are as reported elsewhere.[30]

EXAFS reference data: The EXAFS data were analyzed with experimentally determined reference files obtained from EXAFS data for materials of known structure. The Rh–Rh and $Rh–O_{support}$ interactions were analyzed with phase shifts and backscattering amplitudes obtained from EXAFS data characterizing Rh foil and Rh_2O_3, respectively. The Rh–C and Rh–O* interactions were analyzed with phase shifts and backscattering amplitudes obtained from EXAFS data for crystalline $[Ru_3(CO)_{12}]$ (which has only terminal CO ligands) mixed with BN. $[Ru_3(CO)_{12}]$ was chosen because the multiple scattering effect in the Rh–O* shell is significant as a consequence of the near linearity of the Rh–C–O moieties, and it was necessary to fit the data with a reference that exhibits multiple scattering. The Rh–Na interaction was calculated with the FEFF 4.06 software of Rehr et al.[86] The parameters used to extract these files from the EXAFS data are summarized in Table 9. Details of the preparation of the reference files are presented elsewhere.[78, 90, 91]

Table 9. Crystallographic data characterizing the reference compounds and Fourier transform ranges used in the EXAFS data analysis.[a]

		Crystallographic data			Fourier transform		
Ref. compd	Shell	N	r [Å]	Ref.	Δk, [Å^{-1}]	Δr [Å]	n
Rh foil	Rh–Rh	12	2.687	87	2.86 – 19.60	1.62 – 3.12	3
RhNa[b]	Rh-Na	1	1.75	this work	1.0 – 20.0	0 – 8.0	0
Rh_2O_3	Rh–O	6	2.050	88	2.67 – 15.69	0.00 – 2.10	2
$[Ru_3(CO)_{12}]$	Rh–C	4	1.910	89	3.71 – 14.80	0.95 – 1.87	1
	Rh–O*	4	3.050	89	3.75 – 14.80	1.90 – 3.11	2

[a] Notation: N, coordination number for absorber – backscatterer pair; R, absorber – backscatterer distance; Δk, limits used for forward Fourier transformation (k is the wave vector); Δr, limits used for shell isolation (r is distance); n, power of k used for Fourier transformation. [b] Calculated with FEFF 4.06.[86]

^{13}C and ^{1}H NMR spectroscopy: Magic angle spinning NMR (MAS-NMR) spectra were recorded with a Chemagnetics CMX 400 spectrometer at frequencies of 100.63 MHz for ^{13}C and 400.13 MHz for ^{1}H. Samples were contained in thin-walled glass inserts for 7.5 mm (outside diameter) rotors (Wilmad Glass Co.) that were loaded under N_2 in a glovebox and sealed with epoxy resin. The ^{13}C spectra were typically obtained with a direct excitation spin-echo sequence ($\pi/2$-τ-π-τ-acquire) in order to reduce signal from the NMR-probe assembly, which gave a broad resonance centered near $\delta = 110$ in all spectra. The $\pi/2$ pulse length was 8 μs, and interpulse delays (τ) were set to one rotor period. Spectra were obtained at different spinning frequencies, typically 4.44 and 5.0 k Hz, in order to distinguish centerbands from spinning sidebands. At 25 °C, a relaxation delay of 20 s was used, which corresponds approximately to the spin-lattice relaxation time of the most intense cluster resonance ($\delta = 230$) measured through the inversion – recovery null-point method. These conditions optimized the signal-to-noise ratio at the expense of possible differential saturation effects. At 75 °C, the T_1 of the main cluster resonance ($\delta = 211$) is much shorter, about 1.5 s, than those of the main cluster resonances at 25 °C. The ^{1}H spectra were obtained with single-pulse excitation by use of 90° pulses (8 μs) and 1 – 2 s relaxation delays that allowed for complete relaxation.

Catalysis of toluene hydrogenation by zeolite NaX-supported rhodium clusters: Toluene hydrogenation was catalyzed by zeolite NaX-supported rhodium in a once-through tubular flow reactor mounted in a temperature-controlled Lindberg furnace. Typically, 40 mg of catalyst sample consisting of rhodium carbonyls formed by carbonylation of $[Rh(CO)_2(acac)]$-containing zeolite was diluted with 400 mg of inert α-Al_2O_3 particles and loaded into the reactor to give a bed of catalyst particles 2 – 3 mm in depth. The supported rhodium-carbonyl precursors were treated in flowing He or H_2 at a predetermined temperature to form the catalyst. Toluene was injected into the flow system at a constant rate by an Isco liquid metering pump (Model 260D), and flowed to a vaporizer held at about 140 °C. H_2 flowed through the vaporizer and was mixed with toluene, giving a gas mixture that passed at atmospheric pressure through the reactor at a total flow rate of 46 mL (NTP) min^{-1}. The effluent gas was analyzed with an on-line Hewlett-Packard gas chromatograph (HP-5890 Series II) equipped with a DB-624 capillary column (J&W Scientific) and a flame ionization detector. The catalytic activity was measured at 80, 100, or 120 °C with an H_2 partial pressure of 710 Torr and a toluene partial pressure of 50 Torr. Catalyst samples were typically kept on stream for 8 h.

0947-6539/99/0510-2910 $ 17.50+.50/0 *Chem. Eur. J.* **1999**, *5*, No. 10

EXAFS Data Analysis

Decarbonylated samples formed from rhodium carbonyl-containing zeolite NaX: EXAFS data from 2–6 scans were averaged for each sample (Table 3). The normalized EXAFS functions were obtained from the averaged X-ray absorption spectra by a cubic-spline background subtraction and normalized by division by the edge height (e.g., Figure 12). In the intermediate and higher ranges of the wave vector k ($8 < k < 16$ Å^{-1}), there are strong oscillations characteristic of Rh–Rh interactions in each sample.

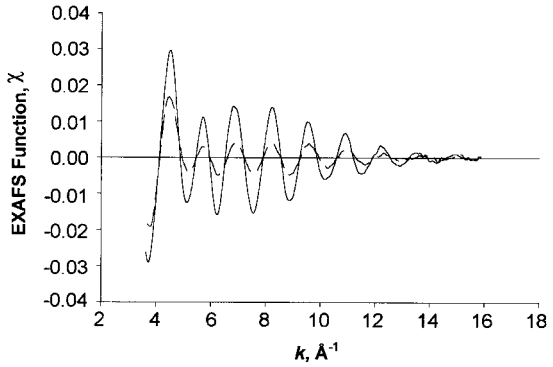

Figure 12. Raw EXAFS data characterizing zeolite NaX-supported rhodium clusters formed from $[Rh(CO)_2(acac)]$ by flowing CO at 125 °C and 2 bar for 12 h followed by decarbonylation in flowing H_2 (solid line) or He at 300 °C (dashed line).

Analysis of the unsmoothed EXAFS data was carried out with a difference file technique.[91, 92] The Rh–Rh contribution, the largest in the EXAFS spectrum, was estimated by calculating an EXAFS function that agreed as closely as possible in r space ($1.5 < r < 3.5$ Å; r is the distance from the absorber atom, Rh) with the k^0-weighted data characterizing the high-k range ($8 < k < 14.6$ Å^{-1}); the metal-support contributions in this high-k range are small because the backscatterers in the support have atomic weights that are low relative to that of Rh. An EXAFS function calculated with the first-guess parameters was subtracted from raw EXAFS data, giving a residual spectrum that was expected to account for Rh–C (representing any residual carbonyl ligands or carbonaceous species resulting from the acac ligands in the precursor $[Rh(CO)_2(acac)]$, Rh–O*, Rh–$O_{support}$, and other Rh-support interactions, that is, Rh–Al, Rh–Na, and Rh–Si). The difference file was estimated with two Rh–O contributions (one characterized by multiple scattering), with another contribution suggested to be Rh–C and yet another to be Rh–Na. All the parameters were varied until good agreement was found between the raw data and the fit with k^0 weighting in r space. At this stage, no attempt was made to fit with higher k weightings. Samples decarbonylated in He were not typically analyzed for a Rh–O* contribution because the infrared spectra indicated the absence of CO ligands on the metal.

The first-guess Rh–Rh and Rh-low-Z backscatterer contributions were then added and compared with the raw data in r space. As the fit was not satisfactory, the Rh-low-Z backscatterer contributions were subtracted from the data, and a better fit for the Rh–Rh contribution was determined. The improved fit characterizing the Rh–Rh contribution was subtracted from the full EXAFS data, and better parameter estimates were determined by fitting the Rh-low-Z backscatterer contributions to the residual spectrum. This process was carried out in r space with the raw EXAFS data with k^0 weighting and repeated until a good overall agreement between the Fourier transform of the raw EXAFS data and the fit in r space was obtained, with the final Rh–Rh contribution showing excellent agreement with the data not only for the k^0 weighting but also for k^1, k^2, and k^3 weightings.

The number of parameters used to fit the data in these main-shell analyses was either 16 or 20. The statistically justified number was approximately 34 for each sample (Table 3); this was estimated on the basis of the Nyquist theorem,[46] $n = (2\Delta k \Delta r/\pi) + 1$, in which Δk and Δr are the k and r ranges used in the forward and inverse Fourier transforms, respectively (Δk and Δr were typically about 10.5 and 5, respectively).

Rhodium carbonyls in zeolite NaX: Analysis of the EXAFS data characterizing the rhodium carbonyls in the zeolite prior to decarbonylation was more complicated than that described above, because there were two Rh–C and two Rh–O* contributions associated with the carbonyl ligands.[93] The positions of the oxygen atoms of the terminal and face-bridging carbonyl ligands in crystalline $[Rh_6(CO)_{15}]^{2-}$ are known.[47] The crystallographic Rh–O* distance characteristic of terminal carbonyl ligands is, on average, 3.00 Å, and the Rh–O* distance characteristic of face-bridging ligands is 3.10 Å. Because the terminal and bridging carbonyl oxygen atoms are located at nearly the same distance from the Rh atom, it is difficult to separate the two contributions in the EXAFS analysis (especially if they are described by similar phase and amplitude functions[92]) and to determine an accurate estimate of the overall Rh–O* coordination number. Because the fitting of the Rh–O* contribution affects the fitting of the Rh–C contributions, there is a discrepancy between the sum of the Rh–C_t and Rh–C_{fb} coordination numbers and the Rh–O* coordination numbers determined by the EXAFS data.

The data representing each of the samples containing the rhodium carbonyls, namely, the samples formed by carbonylation of $[Rh(CO)_2(acac)]$ in uncalcined and in calcined zeolite, were fitted by using one Rh–Rh distance (at about 2.76 Å), one Rh–O distance (at about 3 Å, with multiple scattering), two Rh–C contributions (at distances of about 1.86 and 2.15 Å), and one Rh–Na contribution (at about 4 Å). The number of parameters used to fit the data in these main-shell analyses was 20; the statistically justified number, estimated on the basis of the Nyquist theorem,[46] was approximately 34 for each sample (Table 3).

Acknowledgments

The research was supported by the U.S. Department of Energy, Office of Energy Research, Office of Basic Energy Sciences, Division of Chemical Sciences, contract number FG02-87ER13790. We thank the W. M. Keck Foundation for support to purchase the NMR spectrometer. We acknowledge the Stanford Synchrotron Radiation Laboratory, supported by the Department of Energy, Office of Basic Energy Sciences, for beam time. We also acknowledge the support of the U.S. Department of Energy, Division of Materials Sciences, under contract number DE-FG05-89ER45384, for its role in the operation and development of beam line X-11A at the National Synchrotron Light Source (NSLS). The NSLS is supported by the Department of Energy, Division of Materials Sciences and Division of Chemical Sciences, under Contract No. DE-AC02-76CH00016. We thank the Davison Division of W. R. Grace and Company for providing the zeolite. X-ray absorption data were analyzed with the XDAP software.[96]

[1] P. Gelin, F. Lefebvre, B. Elleuch, C. Naccache, Y. Ben Taarit, *ACS Symp. Ser.* **1983**, *218*, 455.
[2] S. Kawi, B. C. Gates, in *Clusters and Colloids from Theory to Application* (Ed.:G. Schmid) VCH, Weinheim, **1994**, p. 299.
[3] D. De Vos, T. Bein, *J. Am. Chem. Soc.* **1997**, *119*, 9460.
[4] *Oil Gas J.* **1992**, *190*, 29.
[5] Not all the minor peaks can be assigned; some could arise from decomposition of residual pentane solvent and/or acac ligands. The peaks at $\delta = 125$ and 183 are consistent with free CO_2 and CO, respectively.
[6] B. T. Heaton, A. D. C. Towl, *J. Chem. Soc. Chem. Commun.* **1975**, 523.
[7] B. T. Heaton, L. Strona, *J. Organomet. Chem.* **1981**, *215*, 415.
[8] L. S. Bresler, N. A. Buzina, Y. S. Varshavsky, N. V. Kiseleva, T. G. Cherkasova, *J. Organomet. Chem.* **1979**, *171*, 229.
[9] B. T. Heaton, L. Strona, S. Martinengo, D. Strumolo, R. J. Goodfellow, I. H. Sadler, *J. Chem. Soc. Dalton Trans.* **1982**, 1499.
[10] B. T. Heaton, L. Strona, R. D. Pergola, L. Garlaschelli, U. Sartorelli, I. H. Sadler, *J. Chem. Soc. Dalton Trans.* **1983**, 173.
[11] C. Brown, B. T. Heaton, L. Longhetti, W. T. Poley, D. O. Smith, *J. Organomet. Chem.* **1986**, *192*, 93.
[12] J. Evans, B. F. G. Johnson, J. Lewis, T. W. Matheson, J. R. Norton, *J. Chem. Soc. Dalton Trans.* **1978**, 626.
[13] C. Brown, B. T. Heaton, L. Longhetti, D. O. Smith, *J. Organomet. Chem.* **1979**, *169*, 309.

  0947-6539/99/0510-2911 $ 17.50+.50/0

[14] S. Bordoni, B. T. Heaton, C. Seregni, L. Strona, R. J. Goodfellow, M. B. Hursthous, M. Thornton-Pett, S. Martinengo, *J. Chem. Soc. Dalton Trans.* **1988**, 2103.
[15] A. Fumagalli, T. F. Koetzle, F. Takusagawa, P. Chini, S. Martinengo, B. T. Heaton, *J. Am. Chem. Soc.* **1980**, *102*, 1740.
[16] C. Brown, B. T. Heaton, L. Longhetti, W. T. Poley, D. O. Smith, *J. Organomet. Chem.* **1986**, *192*, 93.
[17] P. F. Molitor, R. K. Shoemaker, T. M. Apple, *J. Phys. Chem.* **1989**, *93*, 2891.
[18] N. Takahashi, K. Miura, H. Fukui, H., *J. Phys. Chem.* **1986**, *90*, 2797.
[19] The spectrum shows main peaks at $\delta = 7.7$, 4.0, and 2.4 with smaller shoulders at $\delta = 8.7$, 1.5, 1.1, and 0.3. Spectra taken at 75 °C include these same peaks, although they are much narrower.
[20] V. G. Albano, P. Chini, S. Martinengo, D. J. A. McCaffrey, D. Strumolo, B. T. Heaton, *J. Am. Chem. Soc.* **1974**, *96*, 8106.
[21] Carbido carbon atoms of $[Os_5C(CO)_{14}]^{2-}$ on MgO have been observed by ^{13}C and EXAFS spectroscopies (S. Salvi, G. A. Panjabi, B. L. Phillips, B. C. Gates, unpublished results).
[22] S. Salvi, MS Thesis, University of California, Davis, **1998**.
[23] It was suggested by Brown et al.[16] that because $[Rh_7(CO)_{16}]^{3-}$ is not fluxional at −70 °C but undergoes partial intraexchange at room temperature, some of the terminal carbonyl ligands exchange with some of the edge-bridging CO ligands.
[24] In the fully relaxed single-pulse spectra at 75 °C, the ratio of intensity of the peaks at $\delta = 211$ to those assigned to rhodium subcarbonyls is 4.7(3):1, suggesting a carbon-normalized yield of about 83%. However, this analysis is somewhat uncertain, depending on the origin of the broad, poorly resolved peaks in the 220–300 ppm range, which account for approximately 30% of the total intensity between 150 and 300 ppm.
[25] R. D. Shannon, J. C. Vedrine, C. Naccache, F. Lefebvre, *J. Catal.* **1984**, *88*, 431.
[26] B. E. Hanson, M. E. Davis, D. Taylor, E. Rode, *Inorg. Chem.* **1984**, *23*, 52.
[27] F. Lefebvre, Y. Ben Taarit, *Nouv. J. Chim.* **1984**, *8*, 387.
[28] T. T. Wong, Z. Zhang, W. M. H. Sachtler, *Catal. Lett.* **1990**, *4*, 365.
[29] Similar subcarbonyls of Re on MgO have been fully characterized by infrared and EXAFS spectroscopies and density functional theory: A. Hu, K. M. Neyman, F. M. Staufer, T. Belling, B. C. Gates, N. Rösch, *J. Am. Chem. Soc.* **1999**, *121*, 4522.
[30] W. A. Weber, B. C. Gates, *J. Phys. Chem. B* **1997**, *101*, 10423.
[31] M. E. Davis, E. J. Rode, D. Taylor, B. E. Hanson, *J. Catal.* **1984**, *86*, 67.
[32] E. J. Rode, M. E. Davis, B. E. Hanson, *J. Catal.* **1985**, *96*, 574.
[33] S. Kawi, B. C. Gates, *Inorg. Chem.* **1992**, *31*, 2939.
[34] T. Beutel, S. Kawi, S. K. Purnell, H. Knözinger, B. C. Gates, *J. Phys. Chem.* **1993**, *97*, 7284.
[35] M. Angoletta, L. Malatesta, G. Caglio, *J. Organomet. Chem.* **1975**, *94*, 99.
[36] S. Kawi, J.-R. Chang, B. C. Gates, *J. Am. Chem. Soc.* **1993**, *115*, 4830.
[37] D. M. Vandenberg, T. C. Choy, P. C. Ford, *J. Organomet. Chem.* **1989**, *366*, 257.
[38] S. Kawi, J.-R. Chang, B. C. Gates, *J. Catal.* **1993**, *142*, 585.
[39] A. Zhao, B. C. Gates, *J. Am. Chem. Soc.* **1996**, *118*, 2458.
[40] S. Martinengo, A. Fumagalli, P. Chini, V. G. Albano, G. Ciani, *J. Organomet. Chem.* **1976**, *116*, 333.
[41] A. Fumagalli, S. Martinengo, D. Galli, C. Allevi, G. Ciani, A. Sironi, *Inorg. Chem.* **1990**, *29*, 1408.
[42] S. Martinengo, P. Chini, *Gaz. Chim. Ital.* **1972**, *102*, 344.
[43] J. A. Creighton, R. Della Pergola, B. T. Heaton, S. Martinengo, L. Strona, D. A. Willis, *J. Chem. Soc. Chem. Commun.* **1982**, 864.
[44] The spectra characterizing each of the samples indicate both terminal and face-bridging (but not edge-bridging) CO groups. We infer that these ligands rule out the anionic clusters $[Rh_4(CO)_{11}]^{2-}$ and $[Rh_5(CO)_{15}]^{-}$, which have seven and five edge-bridging CO ligands (with stretching frequencies $> 1800\ cm^{-1}$), respectively, and no face-bridging CO ligands, in contrast to $[Rh_6(CO)_{15}]^{2-}$ and $[Rh_7(CO)_{16}]^{3-}$. Furthermore, the lack of observed edge-bridging CO ligands may suggest the absence of $[Rh_7(CO)_{16}]^{3-}$, because this cluster also has two edge-bridging CO ligands and four face-bridging CO ligands; however, the statement is less strong than the preceding one because the intensity of the bands corresponding to the two edge-bridging CO ligands in $[Rh_7(CO)_{16}]^{3-}$ might be too weak to detect.
[45] Rhodium cations are inferred to be bonded to oxygen atoms of the support and/or to water in the cages.
[46] D. C. Koningsberger, R. Prins (Eds.), *X-Ray Absorption: Principles, Applications, Techniques of EXAFS, SEXAFS, and XANES*, Wiley, New York, **1988**.
[47] V. G. Albano, P. L. Bellon, M. Sansoni, *J. Chem. Soc. A* **1971**, 678.
[48] V. G. Albano, G. Ciani, S. Martinengo, P. Chini, G. Giordano, *J. Organomet. Chem.* **1975**, *88*, 381.
[49] Comparison of the first-shell Rh–Rh coordination number of the rhodium carbonyl clusters supported in calcined and uncalcined zeolite NaX shows a higher coordination number for the uncalcined zeolite. The yield of $[Rh_6(CO)_{15}]^{2-}$ is approximately equal to the Rh–Rh coordination number characterizing the supported cluster divided by the Rh–Rh coordination number of $[Rh_6(CO)_{15}]^{2-}$; thus, the yield of the cluster in the uncalcined sample is estimated to be about 90% and that in the calcined sample about 80%, as calculated on the basis of the Rh–Rh first-shell coordination numbers. The agreement with the values based on NMR intensities is about as good as can be expected.[24] Because the yields in the uncalcined and calcined zeolites differ, it is inferred that the zeolite water may play a role in the $[Rh_6(CO)_{15}]^{2-}$ synthesis.
[50] The migration and subsequent aggregation of transition metal carbonyls supported on metal oxides are illustrated by data characterizing $[Ir_4(CO)_{12}]$ on SiO_2.[51]
[51] R. Psaro, C. Dossi, A. Fusi, R. Della Pergola, L. Garlaschelli, D. Roberto, L. Sordelli, R. Ugo, *J. Chem. Soc. Faraday Trans.* **1992**, *88*, 369.
[52] B. J. Kip, F. B. M. Duivenvoorden, D. C. Koningsberger, R. Prins, *J. Catal.* **1987**, *105*, 26.
[53] D. E. Resasco, R. S. Weber, S. Sakellson, M. McMillan, G. L. Haller, *J. Phys. Chem.* **1988**, *92*, 189.
[54] Reversible oxidative fragmentation-cluster reconstruction has been observed before on surfaces[55]—$[Rh_6(CO)_{16}]$ has been oxidatively fragmented and reversibly reconstructed on the surface of Al_2O_3.[56]
[55] H. H. Lamb, B. C. Gates, H. Knözinger, *Angew. Chem.* **1988**, *100*, 1162; *Angew. Chem. Int. Ed. Engl.* **1988**, *27*, 1127.
[56] A. K. Smith, F. Hugues, A. Theolier, J.-M. Basset, R. Ugo, G. M. Zanderighi, J. L. Bilhou, V. Bilhou-Bougnol, W. F. Graydon, *Inorg. Chem.* **1979**, *18*, 3104.
[57] The formation of coke in zeolites with supported metals is expected and causes deactivation of the metal's hydrogenation activity (V. Fouche, P. Magnoux, M. Guisnet, *Appl. Catal.* **1990**, *58*, 189).
[58] The turnover frequencies were calculated on the basis of the assumption that all the rhodium atoms were surface atoms and therefore accessible. The clusters have six metal atoms or fewer, on average. Therefore, it is likely that all the atoms were accessible to reactants. The largest aggregates are also expected to have had high dispersions (about 80%), as estimated on the basis of the Rh–Rh first-shell coordination numbers. Therefore, errors in the turnover numbers are expected to be small. These assumptions involve neglect of any blockage of rhodium atoms by the support.
[59] W. A. Weber, B. C. Gates, *J. Catal.* **1998**, *180*, 207.
[60] However, because a Rh–Rh first-shell coordination number of about 7 corresponds to a dispersion of about 80%, it follows that the estimates of turnover frequencies are not in error by more than about 25%.
[61] P. Chini, S. Martinengo, *Inorg. Chim. Acta* **1969**, *3*, 315.
[62] L.-F. Rao, A. Fukuoka, N. Kosugi, H. Kuroda, M. Ichikawa, *J. Phys. Chem.* **1990**, *94*, 5317.
[63] P. Chini, S. Martinengo, G. Giordano, *Gaz. Chim. Ital.* **1972**, *102*, 330.
[64] P. Chini, S. Martinengo, *Inorg. Chim. Acta* **1969**, *3*, 299.
[65] S. Martinengo, P. Chini, *Gaz. Chim. Ital.* **1972**, *102*, 344.
[66] S. Martinengo, A. Fumagalli, P. Chini, V. G. Albano, G. Ciani, *J. Organomet. Chem.* **1976**, *116*, 333.
[67] S. Kawi, Z. Xu, B. C. Gates, *Inorg. Chem.* **1994**, *33*, 503.
[68] P. Dufour, L. Huang, A. Choplin, R. Sanchez-Delgado, A. Theolier, J.-M. Basset, *J. Organomet. Chem.* **1988**, *354*, 243.
[69] C. Dossi, R. Psaro, R. Ugo, *J. Organomet. Chem.* **1988**, *353*, 259.
[70] A. M. Liu, T. Shido, M. Ichikawa, *J. Chem. Soc. Chem. Commun.* **1995**, 507.
[71] D. H. Olson, *Zeolites* **1995**, *15*, 439.
[72] Na^+ ions are located in the supercages of NaX zeolite and accessible to the $[Rh_6(CO)_{15}]^2$.

  0947-6539/99/0510-2912 $ 17.50+.50/0

[73] As was hypothesized by Heaton and Towl[6] for $[Rh_6(CO)_{15}]^{2-}$.
[74] Similar shifts have been observed for metal carbonyls in solutions containing Lewis acids such as $Al(C_2H_5)_3$.[75, 76]
[75] D. F. Shriver, *J. Organomet. Chem.* **1975**, *94*, 359.
[76] C. P. Horwitz, D. F. Shriver, *Adv. Organomet. Chem.* **1984**, *23*, 219.
[77] The EXAFS results show strong evidence of a Rh–O contribution at about 2.1 Å. Furthermore, the XANES data suggest that these clusters are slightly electron deficient relative to the bulk metal.
[78] F. B. M. van Zon, S. D. Maloney, B. C. Gates, D. C. Koningsberger, *J. Am. Chem. Soc.* **1993**, *115*, 10317.
[79] Migration of metal carbonyls on hydroxylated metal oxide surfaces has been suggested before.[30, 51]
[80] J. Rathousky, A. Zukal, N. Jaeger, G. Schulz-Ekloff, *Nanostruct. Mater.* **1992**, *1*, 355.
[81] Similar chemistry has been demonstrated for $[Rh_6(CO)_{16}]$ and rhodium subcarbonyls on γ-Al_2O_3.[56]
[82] S. D. Lin, M. A. Vannice, *J. Catal.* **1993**, *143*, 554.
[83] M. Boudart, D. J. Sajkowski, *Faraday Discuss. Chem. Soc.* **1991**, *92*, 57.
[84] F.-S. Xiao, W. A. Weber, O. Alexeev, B. C. Gates, *Proc. 11th Int. Congr. Catal.* (Eds.: J. W. Hightower, W. N. Delgass, E. Iglesia, A. T. Bell), Elsevier, Amsterdam, **1996**, p. 1135; B. C. Gates, in *Catalysis by Di- and Polynuclear Metal Cluster Complexes*, (Ed. R. D. Adams and F. A. Cotton) VCH, Weinheim, **1998**, p. 509.
[85] ICP analysis done at W. R. Grace showed that the zeolite contained 2.1 wt % Rh.
[86] J. J. Rehr, J. Mustre de Leon, S. I. Zabinsky, R. C. Albers, *J. Am. Chem. Soc.* **1991**, *113*, 5135.
[87] R. W. G. Wyckoff, *Crystal Structures, Vol. 1*, 2nd ed., Wiley, New York, **1963**, p. 10.
[88] J. M. D. Coey, *Acta Crystallogr. Sect. B* **1970**, *26*, 1876.
[89] R. Mason, A. I. M. Rae, *J. Chem. Soc. A* **1968**, 778.
[90] J. B. A. D. van Zon, Ph. D. Dissertation, Eindhoven University of Technology, The Netherlands, **1988**.
[91] J. B. A. D. van Zon, D. C. Koningsberger, H. F. J. van't Blik, D. E. Sayers, *J. Chem. Phys.* **1985**, *82*, 5742.
[92] P. S. Kirlin, F. B. M. van Zon, D. C. Koningsberger, B. C. Gates, *J. Phys. Chem.* **1990**, *94*, 8439.
[93] When the Rh–C–O bond angle is greater than approximately 140°, the EXAFS phase shift and amplitude function depend strongly on the positions of the atoms because of multiple scattering effects.[94] In crystalline $[Rh_6(CO)_{15}]^{2-}$, terminal carbonyl ligands have a Rh–C–O bond angle of 176°, and face-bridging carbonyl ligands have a bond angle of 133°.[95] If the same bond angles characterized the rhodium carbonyls in NaX zeolite, then the face-bridging carbonyl ligands would not be expected to show multiple scattering effects. Because of the possibility of cluster interactions with the zeolite wall and neighboring cations, however, there is some uncertainty in these bond angles and the effects of multiple scattering.
[94] F. B. M. van Zon, P. S. Kirlin, B. C. Gates, D. C. Koningsberger, *J. Phys. Chem.* **1989**, *93*, 2218.
[95] E. R. Corey, L. F. Dahl, W. Beck, *J. Chem. Soc. Chem. Commun.* **1963**, 1202.
[96] M. Vaarkamp, J. C. Linders, D. C. Koningsberger, *Physica B* **1995**, *209*, 159.

Received: November 5, 1998
Revised version: March 8, 1999 [F1427]